Journal of Structural Geology 31 (2009) 177–193

Contents lists available at ScienceDirect

Journal of Structural Geology

journal homepage: www.elsevier.com/locate/jsg

Polyphase deformation of the Fuping Complex, Trans-North China Orogen: Structures, SHRIMP U–Pb zircon ages and tectonic implications

Jian Zhang [a], Guochun Zhao [a,*], Sanzhong Li [b], Min Sun [a], Simon A. Wilde [c], Shuwen Liu [d], Changqing Yin [a]

[a] Department of Earth Sciences, James Lee Science Building, The University of Hong Kong, Pokfulam Road, Hong Kong, China
[b] College of Marine Geosciences, Ocean University of China, Qingdao 266003, China
[c] Department of Applied Geology, Curtin University of Technology, Bentley 6012, Western Australia
[d] School of Earth and Space Sciences, Peking University, Beijing 100871, China

ARTICLE INFO

Article history:
Received 6 June 2007
Received in revised form
25 October 2008
Accepted 20 November 2008
Available online 3 December 2008

Keywords:
North China Craton
Archean
Paleoproterozoic
Fuping
Deformation
SHRIMP U–Pb zircon age

ABSTRACT

The Fuping Complex is located in the central part of the Trans-North China Orogen (TNCO), a Paleoproterozoic collisional belt along which the Eastern and Western Blocks were assembled to form the North China Craton. Three stages of deformation (D_1–D_3) have been identified in the Fuping Complex. D_1 formed tight to isoclinal folds F_1, penetrative foliation S_1 and mineral lineation L_1, which resulted from the early NW–SE-orientated thrusting and shearing. D_2 progressively overprinted D_1 and was dominated by mostly NW–SE shortening and top-to-the-SE(E) thrusting under a compressive environment. D_1 and D_2 occurred in association with the peak metamorphism (M_1). D_3 occurred during the exhumation after the crustal thickening, producing regional-scale NWW–SEE-trending open folds (F_3) and associated low-angle detachment faults, and was responsible for the isothermal decompression (M_2) metamorphism of the complex. Following the D_3 deformation, the complex was exhumed to shallow crustal levels where the rocks underwent the retrogressive cooling (M_3) metamorphism.

Syn-tectonic leucocratic dykes are widespread in the Fuping Complex. Two leucocratic dykes that did not experience D_1 but underwent D_2 yield SHRIMP zircon ages of 1843 ± 12 Ma and 1844 ± 18 Ma, which indicate that D_1 must have occurred at some time earlier than ~1844 Ma, whereas D_2 must have occurred at some time later than this age. Two weakly deformed post-D_2 leucocratic dykes yield SHRIMP zircon ages of 1817 ± 14 Ma and 1815 ± 45 Ma, suggesting that the D_2 deformation occurred in the period 1843–1815 Ma. The new SHRIMP data indicate that the collision-related deformation of the Fuping Complex must have occurred in the Paleoproterozoic, not in the late Archean. Structural and geochronological data presented in this study, in association with previous lithological and geochemical data, suggest that the Fuping Complex may have been located in the hinterland of an eastward subduction zone and underwent intensive deformation and metamorphism involved in the final collision between the Western and Eastern Blocks at ~1.85 Ga.

1. Introduction

The Trans-North China Orogen (TNCO) has been interpreted as the site where two discrete continental blocks, called the Eastern and Western Blocks, amalgamated to finally form the coherent basement of the North China Craton (Fig. 1; Zhao et al., 1998, 2001a, 2005; Zhao, 2001; Kusky et al., 2001, 2007; Wilde et al., 2002; Guo et al., 2002, 2005; Polat et al., 2005, 2006; Wilde and Zhao, 2005; Kröner et al., 2005a,b, 2006; Zhang et al., 2007; Li and Kusky, 2007; Faure et al., 2007; Trap et al., 2007). However, controversy exists around the timing and tectonic processes involved in the amalgamation of the two blocks. One school of thought proposed an eastward-directed subduction of an old ocean, with final collision between the two blocks at ~1.85 Ga (Fig. 2a; Wu and Zhong, 1998; Zhao, 2001; Zhao et al., 1998, 1999, 2000a, 2001a, 2007; Wilde et al., 2002; Kröner et al., 2005a,b, 2006; Zhang et al., 2007). In contrast, some others suggested a westward-directed subduction, with final collision between the two blocks to form the North China Craton at ~2.5 Ga (Fig. 2b; Kusky et al., 2001, 2007; Kusky and Li, 2003; Polat et al., 2005; Li and Kusky, 2007). Most recently, Faure et al. (2007) and Trap et al. (2007) proposed another model suggesting a westward subduction with the final collision at 1.9–1.8 Ga (Fig. 2c). To resolve these controversies, it is essential to carry out field-based structural investigations combined with metamorphic, geochemical and geochronological studies in key areas of the TNCO.

* Corresponding author. Tel.: +852 28578203; fax: +852 25176912.
E-mail address: gzhao@hkucc.hku.hk (G. Zhao).

0191-8141/$ – see front matter © 2008 Elsevier Ltd. All rights reserved.
doi:10.1016/j.jsg.2008.11.008

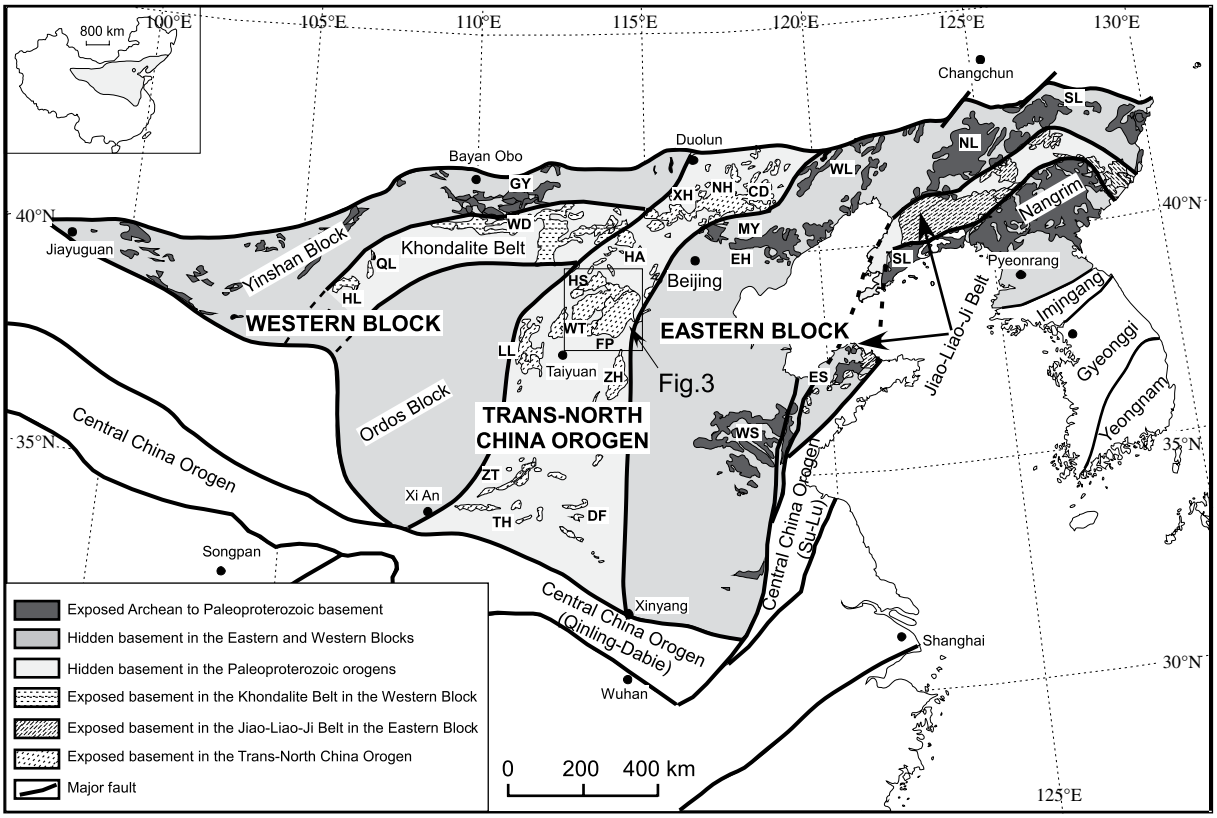

Fig. 1. Tectonic subdivision of the North China Craton (after Zhao et al., 1998, 2001a, 2005), showing the spatial distribution of the basement rocks. Abbreviations for metamorphic complexes: CD – Chengde; DF – Dengfeng; EH – Eastern Hebei; ES – Eastern Shandong; FP – Fuping; GY – Guyang; HA – Huai'an; HL – Helanshan; HS – Hengshan; JN – Jining; LL – Lüliang; MY – Miyun; NH – Northern Hebei; NL – Northern Liaoning; QL – Qianlishan; SJ – Southern Jilin; SL – Southern Liaoning; TH – Taihua; WD – Wulashan-Daqingshan; WL – Western Liaoning; WS – Western Shandong; WT – Wutai; XH – Xuanhua; ZH – Zanhuang; ZT – Zhongtiao.

The Hengshan–Wutai–Fuping region constitutes a lithologically representative transect across the central segment of the TNCO and thus is considered to be the best area for structural, metamorphic and geochronological studies that can be directed towards understanding the tectonic evolution of the TNCO. Of particular significance is the presence of two high-grade gneiss complexes (Fuping and Hengshan Complexes) in the southeast and northwest, respectively, separated by a low-grade granite–greenstone complex (Wutai Complex; Fig. 3). Most recently, Zhang et al. (2007) and Trap et al. (2007) carried out structural investigations on the Hengshan Complex, but they produced contrasting interpretations. Obviously, structural data only from the Hengshan Complex are not enough to reveal the tectonic history of the orogen. Structural data of other complexes and particularly isotopic constraints on the timing of collision-related deformation are very important for further understanding the tectonic evolution of the TNCO. Similar to the Hengshan Complex, the high-grade Fuping Complex also underwent polyphase deformation, pervasive migmatization, and amphibolite- to granulite-facies metamorphism (Zhang et al., 1983; Zhao et al., 2000b; Liu et al., 2002). Therefore, it can provide crucial information on the collisional history of the TNCO. This forms the justification for this study in which we have carried field-based structural investigations on the Fuping Complex. In addition, the Fuping Complex was originally considered as a high-grade gneiss dome resulting from multiple stages of deformation in late Archean (Zhang et al., 1983). To determine the timing of deformation, we carried out SHRIMP U–Pb zircon dating on several syn-tectonic leucocratic dykes (e.g. pegmatite or leucogranitic dykes) that formed at different stages of deformation (e.g. D_2 and D_3). Combined with other geological, geochronological and metamorphic data, these new data provide important insights into understanding the Paleoproterozoic evolution of the TNCO.

2. Geological setting

The North China Craton is the Chinese part of what is used to refer to the Sino-Korea Carton and covers ~1.5 million km^2. The craton can be divided into the Archean to Paleoproterozoic Eastern and Western Blocks, separated by the Paleoproterozoic TNCO (Fig. 1). Lithological, geochemical, structural, metamorphic and geochronological differences between the basements of the Eastern and Western Blocks and the TNCO have been summarized by Zhao et al. (2001a) and references therein. Most recent geological studies have led to further refinement and modification for this three-fold subdivision of the North China Craton. These data suggest that the Western Block was formed by amalgamation between the Yinshan Block in the north and the Ordos Block in the south along the east–west-trending Khondalite Belt at 1.92–1.95 Ga (Fig. 1; Zhao et al., 2005; Xia et al., 2006a,b; Santosh et al., 2006, 2007a,b), whereas the Eastern Block underwent a Paleoproterozoic rifting event along its eastern margin at 2.2–1.9 Ga to form the Jiao-Liao-Ji mobile belt at ~1.9 Ga (Fig. 1; Hao et al., 2004; Luo et al., 2004, 2008; Lu et al., 2006; Li et al., 2006 and references therein; Li and Zhao, 2007).

The TNCO is a nearly south–north trending zone approximately 1200 km long and 100–300 km wide and can be further divided into high-grade complexes and low-grade granite–greenstone complexes. Of these complexes, the Fuping, Wutai and Hengshan Complexes, so called the Hengshan–Wutai–Fuping Mountain Belt, displays a NE–SW trending linear belt transecting the orogen (Fig. 1). The Hengshan Complex is separated from the Wutai Complex by a broad valley of the Hutuo and Sanggan Rivers in the north and northwest, respectively. The Fuping Complex has been recently considered to be in tectonic contact with the Wutai Complex, separated by the Longquanguan ductile shear zone (Fig. 3; Li and Qian, 1991; Zhang et al., 2006), not by a depositional

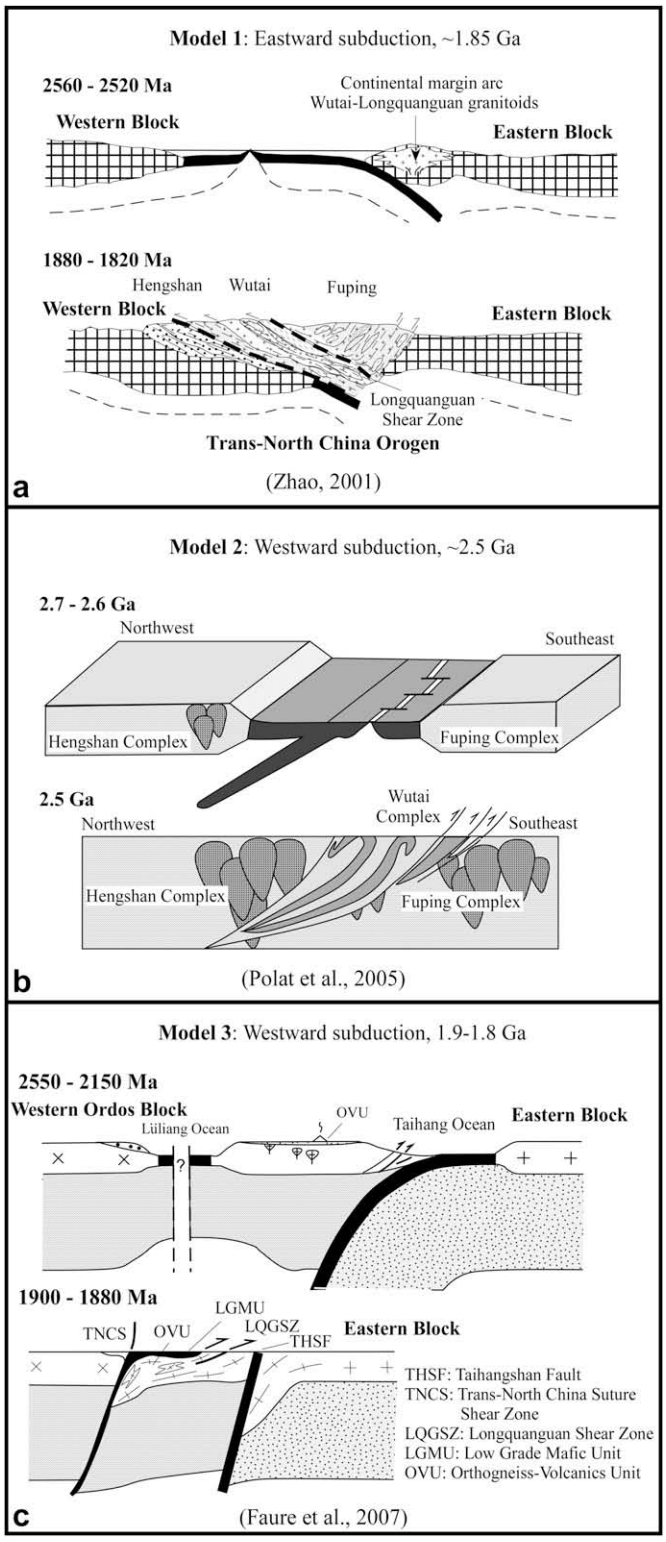

Fig. 2. Recently proposed tectonic models for the tectonic evolution of the TNCO. (a) Eastward subduction models with the final collision at ~1.85 Ga proposed by Zhao et al. (2001a,b, 2007). (b) Westward subduction model with the final collision at ~2.5 Ga, proposed by Polat et al. (2005). (c) Westward subduction model with the final collision at 1.9–1.8 Ga, proposed by Faure et al. (2007).

"unconformity" as previously considered (Bai, 1986; Wu et al., 1989; Tian, 1991).

Based on field-mapping, and lithological, structural and geochronological data, the Fuping Complex can be divided into four distinct lithological units: the Fuping tonalite–trondhjemite–granodiorite (TTG) gneiss, Longquanguan augen gneiss, Wanzi supracurstal assemblage, and Nanying monzogranitic gneiss (Fig. 3; Liu et al., 2000; Zhao et al., 2002). The Fuping TTG gneiss makes up more than ~60% of the total exposure of the complex and consists of medium-grained dioritic, tonalitic, trondhjemitic, granodioritic gneisses, enclosing minor mafic enclaves metamorphosed in the upper amphibolite- and granulite-facies (e.g. mafic granulites, amphibolites and hornblende gneisses). SHRIMP U–Pb zircon data indicate that the Fuping TTG gneiss was emplaced simultaneously with the Hengshan TTG gneiss at 2520–2475 Ma (Guan et al., 2002; Zhao et al., 2002; Kröner et al., 2005a,b, 2006).

The Longquanguan augen gneiss is composed predominantly of mylonitized granodioritic and monzogranitic gneisses and restricted to the Longquanguan and Ciyu-Xinzhuang ductile shear zones (Fig. 3). The augen gneiss was previously interpreted as the youngest lithological unit in the Fuping Complex (Liu et al., 1985). However, recent SHRIMP U–Pb zircon ages revealed that the Longquanguan augen gneiss was emplaced at ~2540 Ma (Wilde et al., 1997), broadly simultaneous with the 2560–2520 Ma Wutai gneissic granites, but older than the 2520–2480 Ma Fuping TTG gneiss (Wilde et al., 1997). Therefore, the Longquanguan augen gneiss most likely represents the equivalent of the Wutai granites but was structurally reworked during the development of the Longquanguan ductile shear zones.

The Wanzi supracrustal assemblage extends along a 100 km long, NE–SW trending belt in the southern part of the complex (Fig. 3), and comprises pelitic gneisses, pelitic schists, calc-silicate rocks, pure and impure marbles and amphibolites that are metamorphosed in amphibolite facies (Liu and Liang, 1997; Zhao et al., 2000b, 2002). The Wanzi supracrustal assemblage was previously considered to have been deposited between 2800 and 2560 Ma (Liu et al., 1985), but recent SHRIMP zircon data indicate that the deposition of the Wanzi supracrustal assemblage occurred at some time between 2100 and 1860 Ma (Zhao et al., 2002). Associated with the supracrustal rocks are some sillimanite-bearing granites, which are considered as S-type granites derived from partial melting of pelitic gneisses (Zhao et al., 2000b, 2002).

The Nanying monzogranitic gneiss consists of medium- to fine-grained, weakly foliated, magnetite-bearing monzogranitic and granodioritic gneisses (Fig. 3; Liu et al., 2002; Zhao et al., 2000b, 2002). Regionally, the Nanying gneiss intrudes the Fuping TTG gneiss, whereas in the places where the contact relations are preserved, the Nanying and Fuping gneisses display the uniform penetrative foliations and folded patterns, suggesting that they were most likely to have undergone the same stages of deformation. Recent SHRIMP data showed that the protolith of the Nanying monzogranitic gneiss was emplaced in the period 2077–2024 Ma (Guan et al., 2002; Zhao et al., 2002).

In addition to the above four major lithologies, there are abundant deformed and undeformed granitic or pegmatoid dykes in the Fuping complex. Two undeformed pegmatitic dykes yielded a SHRIMP zircon age of 1790 ± 8 Ma (Wilde et al., 1998) and a TIMS zircon age of 1799 ± 9 Ma (Liu et al., 2000), suggesting that the major deformational events must have occurred before ~1800 Ma. This conclusion is further supported by $^{40}Ar/^{39}Ar$ ages of 1774.7 ± 0.7 Ma and 1780.7 ± 0.5 Ma obtained for unmetamorphosed mafic dykes in the Zanhuang Complex (ZH in Fig. 1; Wang et al., 2003, 2004a), more than 10 km southeast of the Fuping Complex. However, those deformed granitic or pegmatoid dykes have not been well dated.

Metamorphic history of the Fuping Complex has been studied in detail on the mafic granulites (now preserved as mafic boudins or enclaves in the TTG gneiss) and metapelitic gneisses (Zhao et al., 2000b; Liu and Liang, 1997). Three distinct metamorphic stages have been recognized from the Fuping mafic granulites (Fig. 4a; Zhao

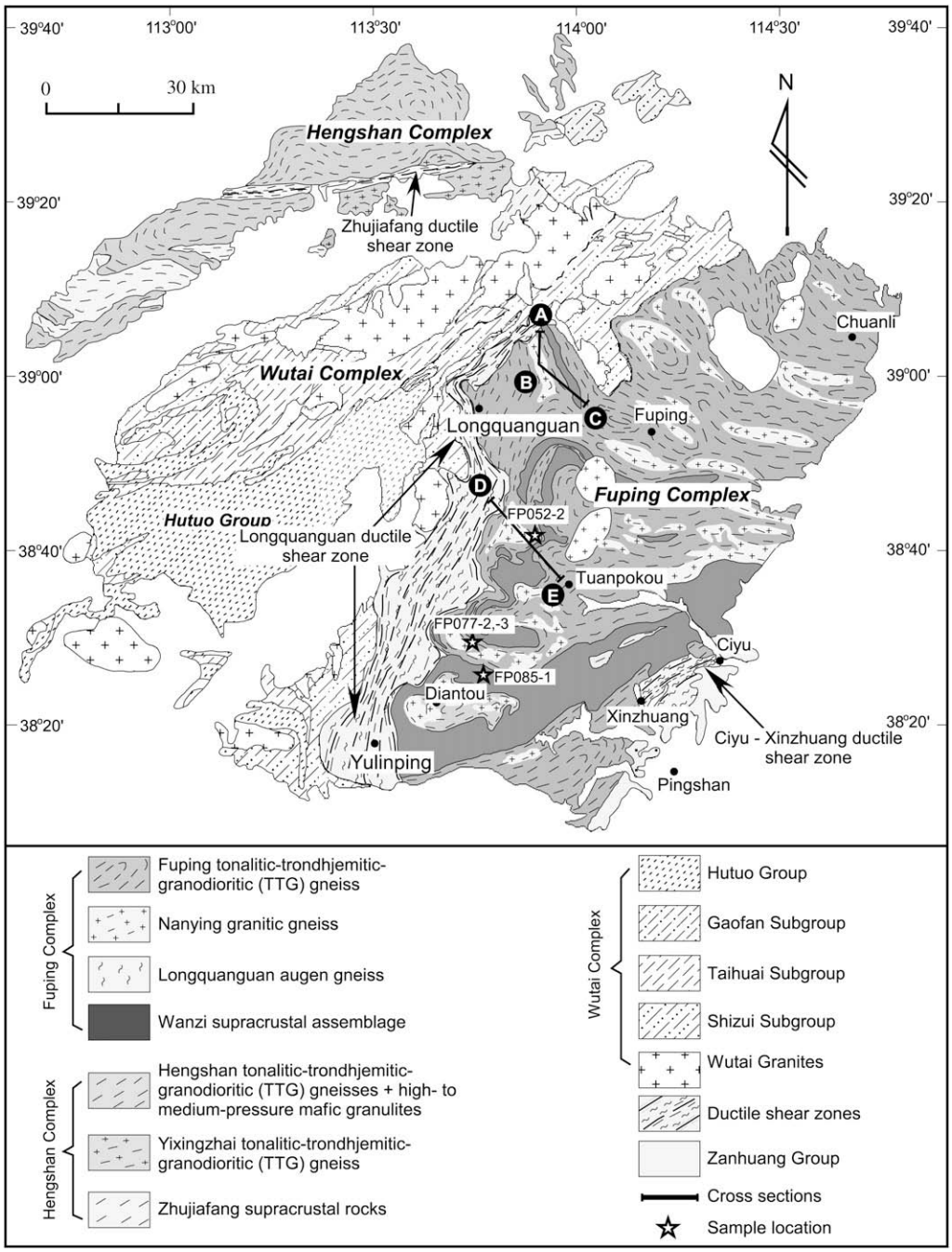

Fig. 3. Geological map of the Fuping, Wutai and Hengshan Complexes, showing spatial relationships and major lithological units (after Liu et al., 2000; Zhao et al., 2000b).

et al., 2000b): peak (M_1), decompression (M_2) and late cooling and retrogression (M_3). The peak metamorphism (M_1) is presented by the mineral assemblage of garnet porphyroblasts and orthopyroxene + clinopyroxene + plagioclase + quartz + hornblende ± biotite, with P–T conditions of 8.0–8.5 kbar and 900–950 °C (Zhao et al., 2000b). The decompression metamorphism (M_2) is indicated by orthopyroxene + plagioclase symplectites and clinopyroxene + plagioclase ± orthopyroxene coronas, formed at P–T conditions of 6.0–7.0 kbar and 700–800 °C (Zhao et al., 2000b). The late cooling and retrograde metamorphism (M_3) formed the Hbl + Pl symplectites at P–T conditions of 5.3–6.3 kbar and 550–650 °C (Zhao et al., 2000b). These mineral assemblages and their P–T conditions defined a clockwise P–T path involving near-isothermal decompression (Fig. 4a). A similar P–T path was also reconstructed for the metapelitic gneisses of the Fuping Complex (Fig. 4b; Liu and Liang, 1997). These P–T paths suggest that the Fuping Complex underwent a tectonothermal process that was characterized by initial crustal thickening, followed by exhumation and cooling, which was considered to have recorded the tectonothermal history involved in the collision between the Eastern and Western Blocks (Zhao et al., 2000a,b).

3. Structural history

The structural style of the complex is dominated by composite folding and shearing (Fig. 5). In order to determine the structural pattern of the complex, we carried out two structural cross-sections in the northern and southern part, respectively. Based on

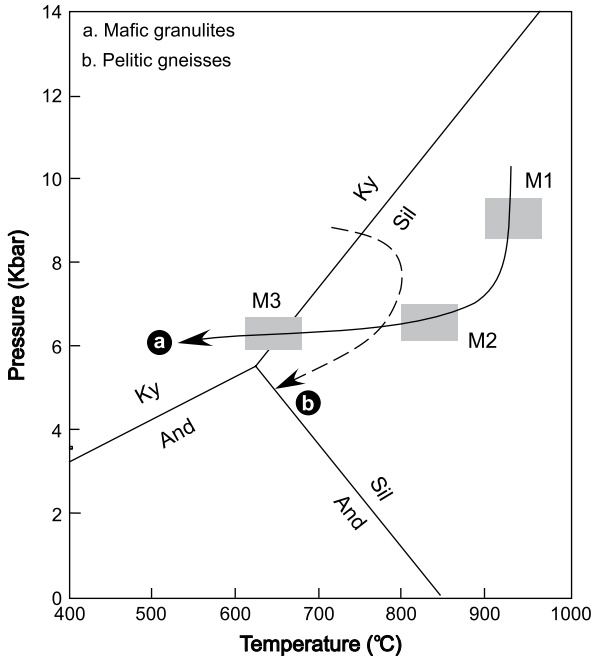

Fig. 4. Metamorphic P–T paths. (a) P–T path of the Fuping mafic granulites (Zhao et al., 2000b). (b) P–T path of the metapelitic gneisses (Liu and Liang, 1997).

the overprinting and geometric observations, three stages of deformation (D_1–D_3) were identified. Although the structural fabrics display variable geometrical and kinematic complexity, they record a progressive transition from the early ductile deformation (D_1–D_2) associated with the peak metamorphism, through semi-ductile to brittle deformation (D_3) associated with post-peak exhumation. Detailed major structural features for different deformational stages are described below.

3.1. Deformation D_1

The earliest D_1 fabrics are characterized by isoclinal folds F_1, and associated axial planar foliation S_1 and mineral lineation L_1. The F_1 isoclinal folds are rarely preserved due to intensive reworking of later deformation. In the field, the F_1 folds are restrictedly preserved in the mafic and metapelitic rocks (Fig. 6a, c). S_1 is defined by orientated platy minerals in the supracrustal rocks, or by felsic ribbons with oriented biotites in the migmatized TTG gneiss. Regionally, the S_1 foliations show moderate to shallow dipping angles and display variable orientations due to the later stages of deformation (Fig. 7, D_1). On the S_1 plane, the L_1 lineation is outlined by a preferred orientation of syn-kinematic clinopyroxene or hornblende aggregates (Fig. 6b). In some localities where the S_1 foliation has been completely overprinted by the subsequent D_2 deformation, the stretching lineation observed on the fold limbs mostly represents the newly developed L_2 lineation. Therefore, the measurements of the L_1 lineations are strictly localized on those S_1 foliations that are less transposed by the S_2 foliations. As shown on the stereonet projections, although the S_1 foliations have been folded to various orientations, most of the L_1 mineral stretching lineations measured on S_1 display a preferred NW-SE plunging orientation at shallow angles (Fig. 7, D_1), indicating an NW–SE-oriented sense of thrusting and shearing.

3.2. Deformation D_2

The D_2 deformation progressively overprinted the D_1 fabrics and formed kilometer- to meter-scale, tight to isoclinal folds F_2 and associated axial planar to penetrative foliations S_2. All the earlier D_1 fabrics in the granitoid genisses and supracrustal rocks of the Fuping Complex were affected by the D_2 deformation. A successive overprinting relationship between the D_2 and D_1 deformation can be locally observed in meter-scale outcrops, where the earlier F_1 isoclinally folded calc-silicates and amphibolites have been successively refolded by the F_2 folds (Fig. 6c and d).

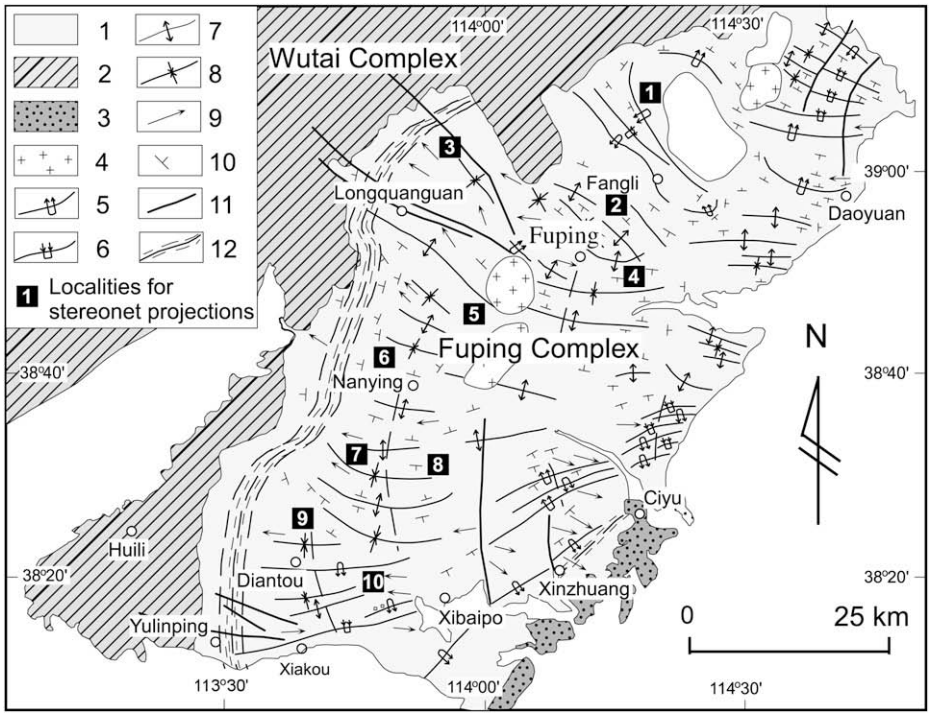

Fig. 5. Detailed structural sketch map of the Fuping Complex, revised after Zhang et al. (1983) and Wu et al. (1989). 1, Fuping Complex; 2, Wutai Complex; 3, Paleoproterozoic Zanhuang Group; 4, Mesozoic granites; 5, F_2 isoclinal folds or closed antiforms; 6, F_2 isoclinal folds or tight synforms; 7, F_3 upright open antiforms; 8, F_3 upright open synforms; 9, mineral lineation (L_1/L_2); 10, penetrative foliation (S_1/S_2); 11, major faults; 12, ductile shear zone.

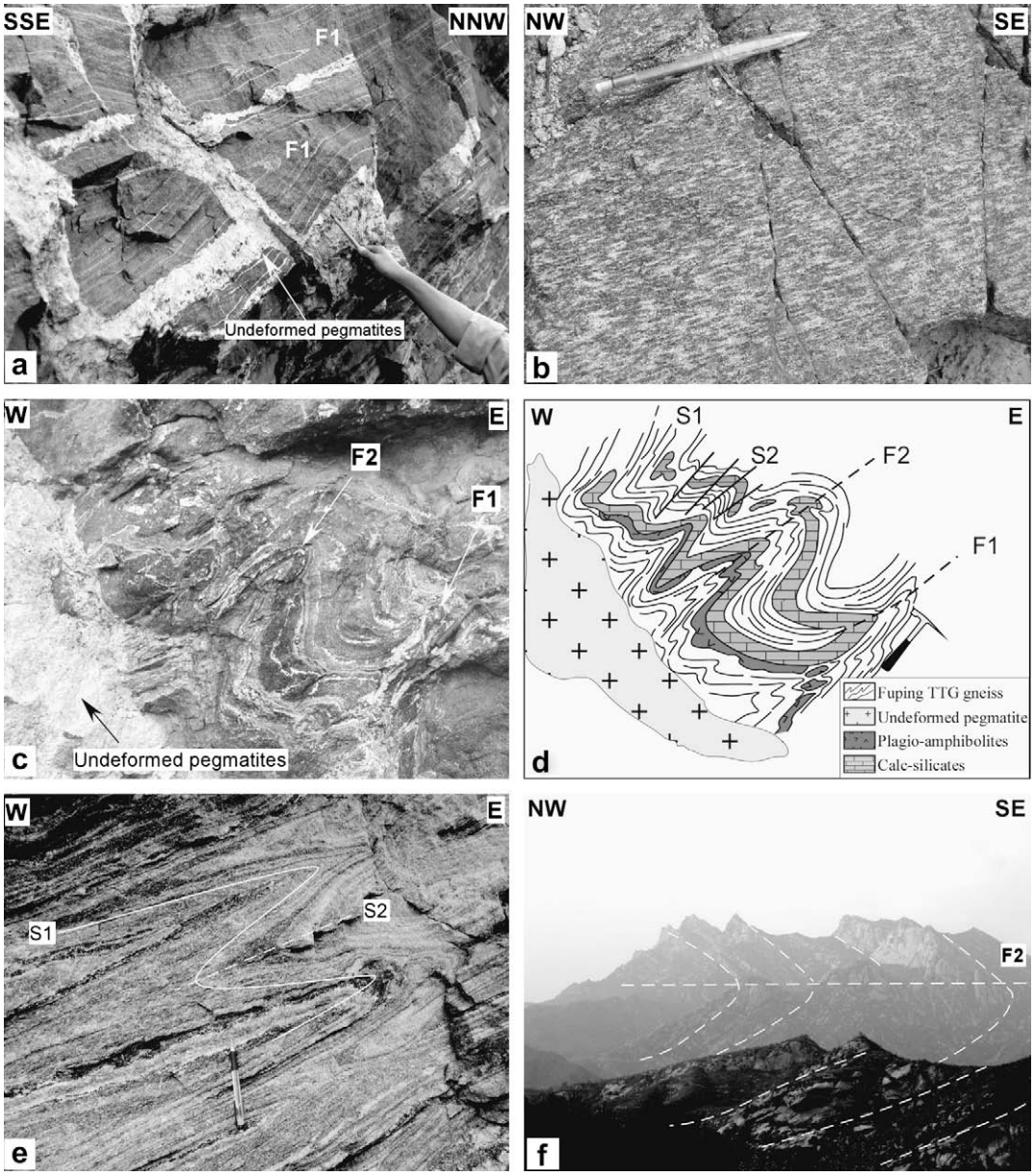

Fig. 6. Field photos showing typical structural fabrics associated with D_1 and D_2. (a) F_1 isoclinal folds preserved in the mafic rocks (plagio-amphibolites). (b) L_1 stretching lineation (aggregates of hornblende) on the S_1 gneissic foliations indicate a NW–SE plunging orientation. (c) Progressively overprinting relationship between the F_2 and F_1 folds preserved in supracrustal rocks. (d) A sketch for the outcrop photo Fig. 7c, illustrating a progressively overprinting relationship between the F_2 and F_1 folds. (e) In highly deformed localities, F_2 isoclinal folds have transposed S_1 foliation to be S_2. (f) SE-verging large-scale F_2 recumbent folds with horizontal fold axial plane in the southern Fuping Complex.

The D_2 fabrics are pervasively distributed in the Fuping Complex. The D_2 deformation is characterized by the asymmetric, overturned to recumbent F_2 folds of variable scales and associated thrust faults (Figs. 6f and 8), indicating a top-to-the-SSE or E sense of thrusting. Locally, the F_2 folds have significantly thickened hinge zones and thinned and sheared limbs (Fig. 6e). In places the F_2 folds are dominantly tight to isoclinal, the S_1 foliations have been intensively folded and transposed to the newly developed penetrative S_2 foliations (Fig. 6e). S_2 is sub-parallel to the S_1 foliation in the limbs of F_2 and intersects with S_1 at a high angle in the hinge zones (Fig. 6e). The S_2 foliations generally display shallow dips, but become much steeper in the localities that were refolded by the subsequent F_3 upright open folds (Fig. 7, D_2 and D_3; Fig. 8). Regionally, except in the northern part of the Fuping Complex where the F_2 fold axes plunge to WNW, most of the F_2 fold axes plunge to SW–NE (Fig. 7, D_2 and D_3), indicating a mostly NW–SE-oriented shortening during D_2.

Numerous mafic boudins and lenses of granulites and amphibolites outcrop within the Fuping TTG genisses. In low-strain zones, these mafic boudins and lenses can be traced up to several hundred meters in length, which suggests that they were derived from mafic dykes. Ductile deformation has later rotated these dykes into parallelism with the layering in the enclosing gneisses and, at the same time, caused boudinage (Fig. 9a). Petrographic examination has revealed that these mafic boudins are mostly composed of granulite-facies orthopyroxene + clinopyroxene + plagioclase in their cores and amphibolites-facies plagioclase + hornblende in their rims (Zhao et al., 2000b). These observations suggest that these pre-existed mafic dykes underwent intensive stretching, rotating and shearing deformation during D_2 and experienced the amphibolite- to granulite-facies metamorphism.

Associated with the D_2 deformation was the development of the Longquanguan ductile shear zone that extends as a NE–SW

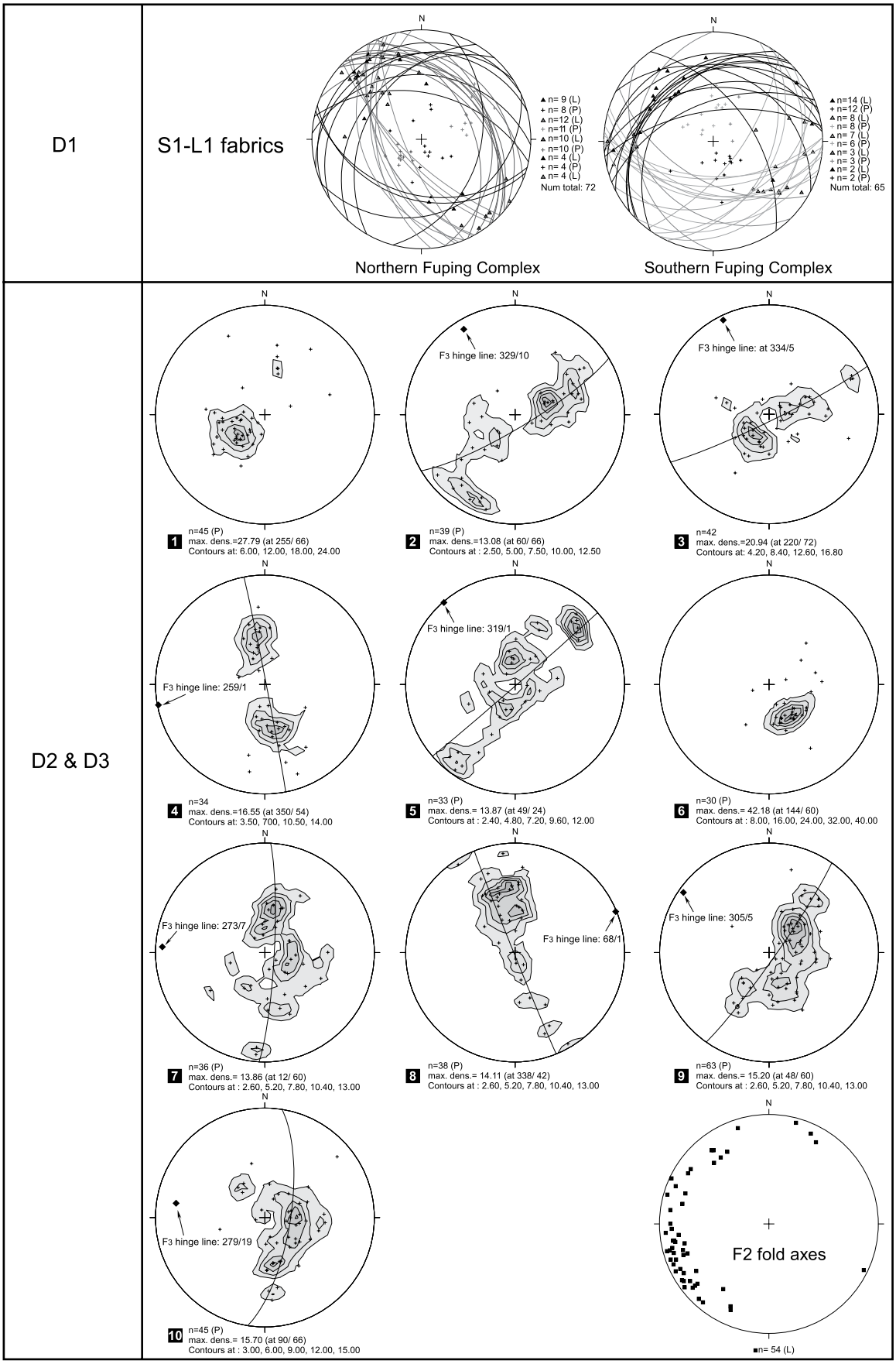

Fig. 7. Stereonet projections (lower hemisphere equal-area projection) showing the attitudes of the D_1, D_2 and D_3 composite fabrics in different metamorphosed areas of the Fuping Complex. In D_1, although S_1 foliations were refolded to different attitudes, L_1 stretching lineations display the preferred NW–SE orientation. In D_2 and D_3, S_2 foliations were refolded by nearly NW–SE trending F_3 open folds. Measurements for S_2 foliations are F_2 fold axial planes, S_2 crenulation cleavages and F_2 isoclinal fold limbs.

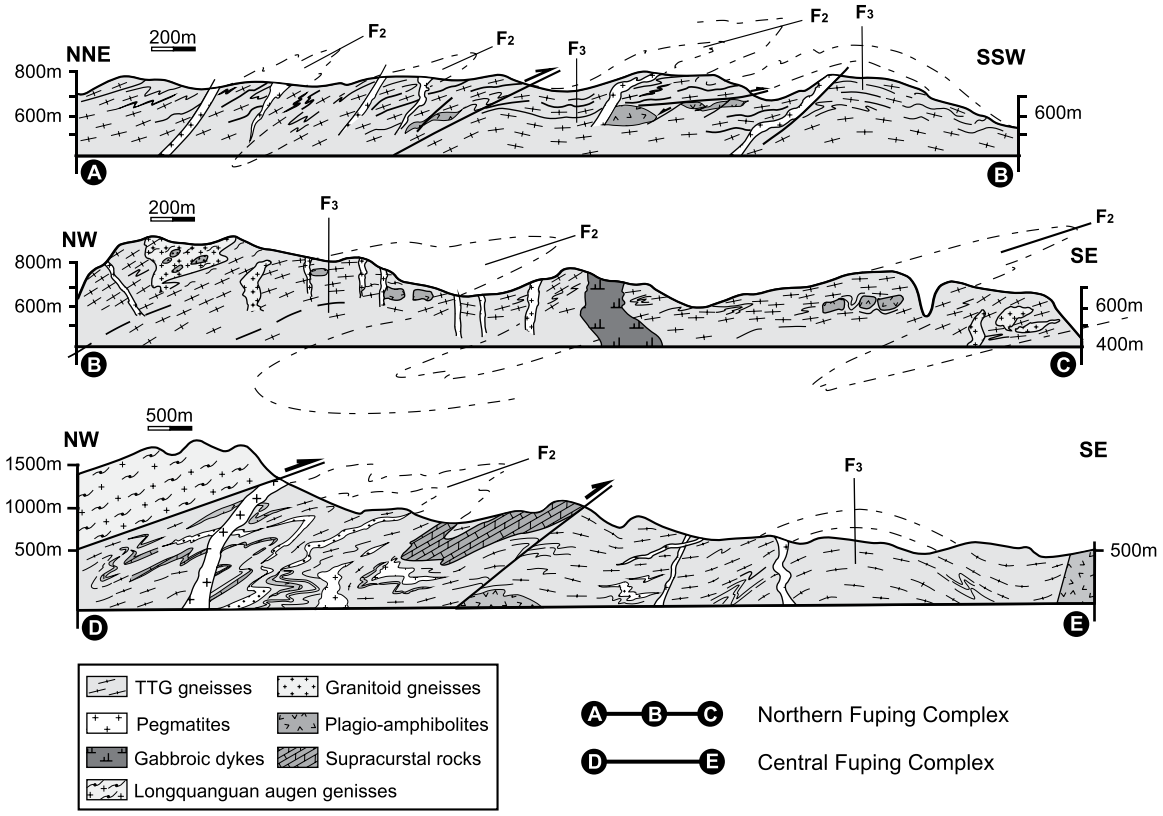

Fig. 8. Structural cross-sections of the Fuping Complex. Cross-section ABC is characterized by the SE-verging, overturned to recumbent F_2 folds and thrust faults, indicating a top-to-the-SE thrusting. F_3 upright open folds refolded the D_2 fabrics to be antiforms. Cross-section DE shows a similar structural pattern with ABC, consisting of the highly deformed Longquanguan augen gneiss and the TTG gneiss, SE-verging overturned to recumbent F_2 folds and F_3 upright open folds. Syn and post-tectonic leucocatic dykes are both preserved in the Fuping lithologies. Section lines are shown in Fig. 3.

trending belt along the boundary between the Fuping and Wutai Complexes (Figs. 3 and 5). The Longquanguan ductile shear zone is characterized by augen gneisses that were tectonically reworked and thrust onto the other Fuping lithologies (Fig. 8, Cross-section DE). In the areas adjacent to the ductile shear zone, the Fuping TTG gneiss and supracrustal rocks have been intensively refolded, forming structures consistent with those of the Longquanguan augen gneiss (Fig. 9b). In the interior of the shear zones, mylonitic foliations strike NNE–SSW and dip shallowly to W and NW (Fig. 5). The kinematic indicators (e.g. S–C structure, σ-augen or drag folds) in the ductile shear zone pervasively indicate a top-to-the-SE(E) sense of shearing and thrusting (Fig. 9c). This suggests that the Lonquanguan ductile shear zone mostly developed during the D_2 deformation and along this shear zone, parts of the Wutai granite–greenstone sequences were thrust southeastwards onto the Fuping Complex.

3.3. Deformation D_3

The D_3 deformation generated large-scale semi-ductile (e.g. open folds F_3 and crenulation cleavages S_3) to brittle (e.g. slip bands or detachment faults) structures in the Fuping Complex. Semi-ductile structures are characterized by large-scale open folds F_3 that refolded the earlier D_1 and D_2 fabrics, causing a wide range of orientations of the F_2 fold axes (Fig. 7, D_2 and D_3). Since the F_3 folds are mostly large-scale open folds and do not have penetrative axial plane foliations, the F_3 fold hinges can be traced by measuring and projecting the attitudes of the bilateral F_3 fold limbs on the stereonet (Fig. 7, D_2 and D_3). The F_3 fold axes generally exhibit a NWW–SEE trend that is different from the orientation of the F_2 fold axes, and thus the superimposition of F_3 on F_2 resulted in the regional-scale dome-and-basin interference patterns in the area (Figs. 3 and 8). In the hinge zones of F_3, anatectic felsic veins or dykes are commonly present along the S_3 cleavages (Fig. 9d), indicating that the D_3 deformation was associated with partial melting that occurred at the decompression/exhumation stage (M_2). In other places where the S_3 cleavages are rarely developed, brittle structures are present. As shown in Fig. 9e, the TTG gneiss and leucocratic veins surrounding the mafic boudins were slightly bent by the F_3 folds and transposed to be the brittle slip fabrics. Associated with the D_3 deformation was the development of meso-to-regional-scale low-angle detachment faults (Fig. 9f) that are widespread in the different lithological units (e.g. gneisses, supracrustal rocks and mafic dykes) of the Fuping Complex. Similar structures were also observed in the Longquanguan ductile shear zone and interpreted as exhumation-related collapse structures by Zhang et al. (2006). These observations suggest that the D_3 deformation occurred under an extensional environment, most possibly related to the exhumation following the crustal thickening.

4. SHRIMP U–Pb zircon geochronology

Abundant syn-tectonic leucocratic granites and pegmatites have been recognized in the Fuping Complex (Fig. 10). They are characterized by sheets, dykes and veins of granite and pegmatite, most of which are slightly to grossly discordant to the gneissic foliation. In general, these dykes display syn- or post-tectonic structural relationships to the host gneissic foliation, and thus their ages can be used to approximately constrain the timing of the major stages of deformation. In this section, we use the SHRIMP U–Pb zircon dating

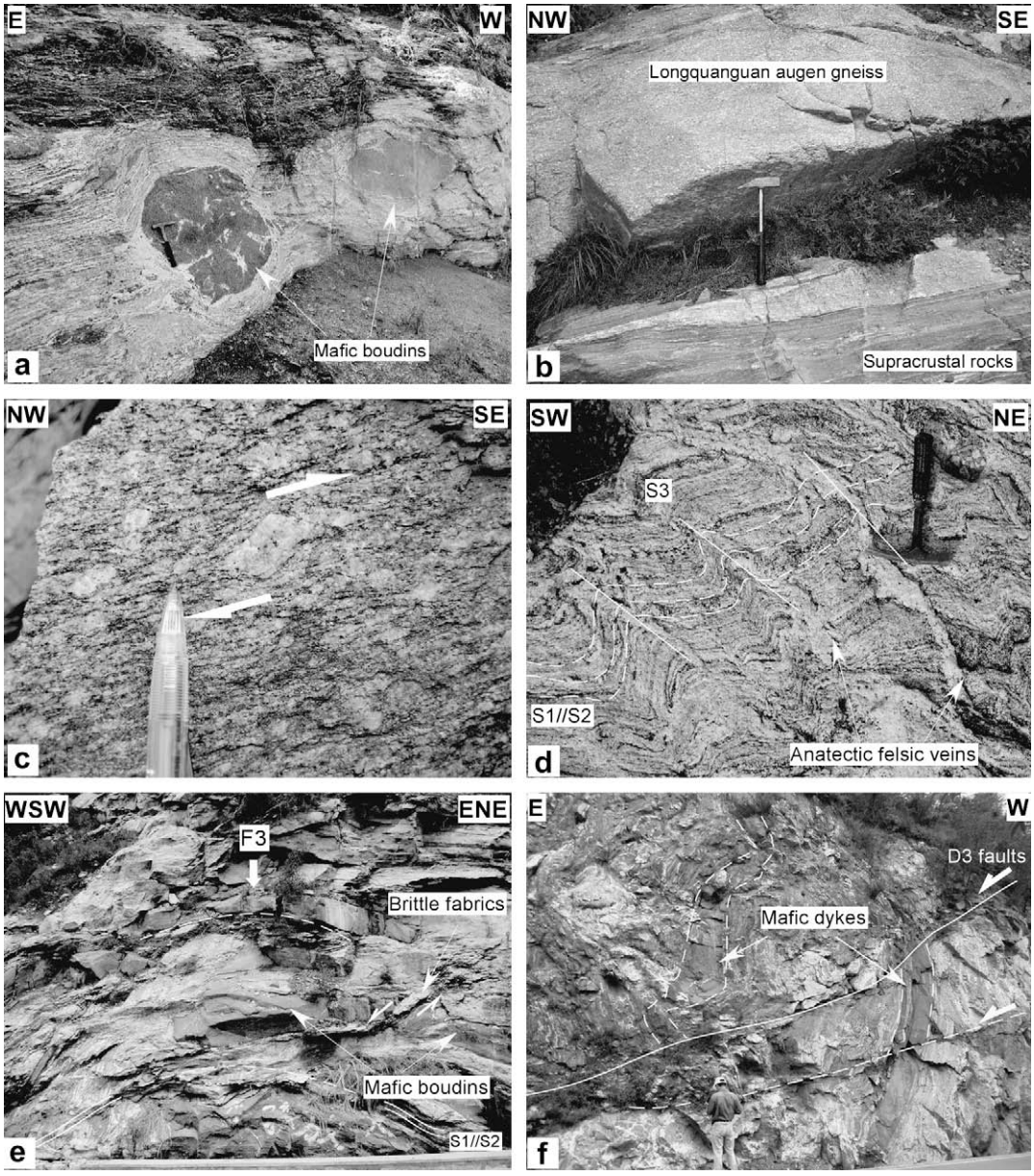

Fig. 9. Field photos showing typical structural fabrics associated with D_2 and D_3. (a) Mafic boudins (granulites and amphibolites) are surrounded by highly deformed TTG gneiss. (b) Longquanguan augen gneiss shows similar structures with the Fuping supracrustal rocks. (c) σ-type augen preserved in the Longquanguan augen gneiss indicating a top-to-the-SE shearing. (d) In the hinge zones of F_3, anatectic felsic veins or dykes are commonly present along the S_3 cleavages. (e) F_3 upright open folds refolding the earlier D_1 and D_2 fabrics. Note brittle slip bands along the boundaries between the boudinaged mafic dykes and the Fuping TTG gneiss. (f) D_3 low-angle normal faults, reworking the pre-existed Fuping lithologies and D_1–D_2 fabrics.

technique to determine the ages of the leucocratic granite and pegmatite dykes. The locations of the studied samples are shown in Fig. 3.

4.1. Analytical techniques

The samples were processed by crushing and initial heavy liquid and subsequent magnetic separation. Zircons extracted from the samples were hand picked and mounted onto double-sided adhesive tape and then enclosed in epoxy resin surface. After drying, the epoxy resin surface was ground and polished to cut all zircon grains in half size. Each sample was then photographed in both transmitted and reflected light in order to enable grain identification during analysis. Cathodoluminescence (CL) images were used to identify possible internal structural complexities and to ensure that analytical sites did not transgress internal boundaries. U–Th–Pb analyses of the zircons were conducted using the WA Consortium SHRIMP II ion microprobe housed at Curtin University of Technology, following operating procedures described by Williams (1998). Isotopic ratios were monitored by reference to Sri Lankan gem zircon standard (CZ3) with a $^{206}Pb/^{238}U$ ratio of 0.0914 that is equivalent to an age of 564 Ma (Pidgeon et al., 1994). Pb/U ratios in the unknown samples were corrected using the ln(Pb/U)/ln(UO/U) relationship as measured in standard CZ3. Ages have been calculated from the U and Th decay constants recommended by Steiger and Jäger (1977). All reported ages represent $^{207}Pb/^{206}Pb$ data that have been corrected using measured ^{204}Pb. The analytical data were reduced, calculated and plotted using the Squid (1.0) and IsoplotEx 2.46 programs (Ludwig, 2001). Individual analyses in the data table and concordia plots are presented as 1σ error boxes and

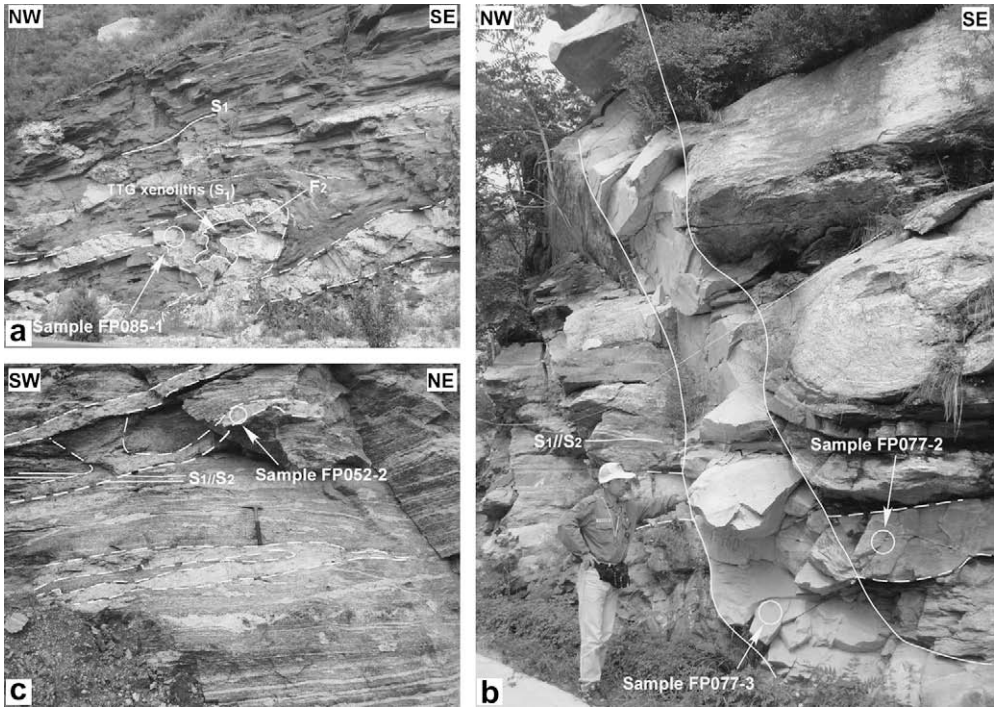

Fig. 10. Outcrop photos showing syn-tectonic leucocratic dykes. (a) A F_2-folded pegmatite dyke (FP085-1) intrudes the Fuping TTG gneiss and encloses the xenoliths of the host deformed TTG gneiss at the hinge zones, indicating that it was emplaced into the TTG gneiss after the D_1 deformation and underwent the subsequent D_2 deformation. (b) A deformed fine-grained leucogranitic dyke (FP077-2) shows penetrative S_2 foliations parallel to the host gneisses, indicating that its emplacement pre-dated the D_2 deformation. A weakly deformed coarse-grained leucogranitic dyke (FP077-3) truncates the dyke FP077-2 and S_2 foliations, suggesting its emplacement post-dated the D_2 deformation. (c) A weakly deformed pegmatite dyke (FP052-2) intrudes the host TTG gneisses and displays discordant structures with host S_2 gneissic foliations.

uncertainties in ages are quoted at the 2σ(95 percent confidence) level, unless otherwise indicated.

4.2. Analytical results

4.2.1. Sample FP085-1

Sample FP085-1 was collected from a tightly folded muscovite–biotite-bearing granitic pegmatite dyke (lat. N38°29.424′; long. E113°44.379′) that intrudes the Fuping TTG gneiss in the central part of the Fuping Complex (Fig. 3). The pegmatite dyke and the felsic veins in the host TTG gneiss have been refolded to be 'Z' type asymmetric folds F_2 (Fig. 10a). The fold limb is sub-parallel to the host TTG gneissic foliation, whereas in the fold hinge the pegmatite dyke becomes thicker and encloses a xenolith of the deformed TTG gneiss with a S_1 foliation (Fig. 10a). The F_2 axial plane shallowly dips to the WNW, coherent with the attitudes of the regional S_2 foliation. Observed in the thin sections, the pegmatite dyke is coarse-grained and consists of plagioclase (50%), K-feldspar (15%), quartz (20%), muscovite (5%) and biotite (5%) and shows a blastogranitic texture in which large, tabular igneous plagioclases exist with small subhedral quartz, plagioclase and K-fieldspar grains with triple-junction textures (Fig. 11a), indicating that the dyke has undergone metamorphism. Taken together, these features suggest that the pegmatite dyke was most possibly emplaced into the TTG gneiss after the D_1 deformation and then underwent the subsequent D_2 deformation together with the host TTG gneiss.

Zircons from the sample are prismatic and large in grain size (400–500 μm). The CL images show that most zircons in the dyke have a wide concentrically oscillatory zoning core (Fig. 12a, b, c), typical of magmatic origin, and a narrow nebulously zoned rim (Fig. 12a, b), possibly resulting from late-stage hydrothermal alteration. Of ten analyses, four were made on the oscillatory zoning cores and six on narrow nebulously zoned rims, but on the Concordia diagram (Fig. 13a), all data-points show similar apparent $^{206}Pb/^{207}Pb$ ages ranging from 1800 to 1884 Ma, most of which are discordant (Table 1 and Fig. 13a). A York regression through the 10 data-points, using IsoplotEx, defines an upper intercept age of 1843 ± 12 Ma (MSWD = 1.14), interpreted as the magmatic crystallization age of the pegmatite dyke.

4.2.2. Samples FP077-2 and FP077-3

Samples FP077-2 and FP077-3 were collected from two granitic dykes in the central part of the Fuping Complex (lat. N38°35.753′; long. E113°43.725′) (Fig. 3). These dykes also intrude the Fuping TTG and Nanying monzogranitic gneisses but show different structural relationships to the host gneisses (Fig. 10b). Sample FP077-2 was collected from a relatively early leucogranitic dyke that intrudes the TTG gneiss and displays deformational fabrics coherent with the foliation of the TTG gneiss (S_2), suggesting that it was emplaced at some time before or synchronously with the D_2 deformation, whereas Sample FP077-3 was collected from a younger weakly deformed leucogranitic dyke that truncates both of the older deformed dyke and host gneissic S_2 foliations (Fig. 10b), suggesting that its emplacement post-dated the D_2 deformation.

Sample FP077-2 is composed of fine-grained K-feldspar (40%), plagioclase (30%), quartz (15%), biotite (10%) and muscovite (5%). In thin sections, minerals do not exhibit strong evidence of subsolidus plastic strain and preserve a blastogranitic texture where biotite flakes show an orientated gneissic foliation (Fig. 11b). K-feldspar occurs as elongate (length-to-width ratio of 2:1) anhedral crystals parallel to the biotite foliation (Fig. 11b). In some places, K-feldspar, plagioclase and quartz grains form a triple-junction texture (Fig. 11b). These features show that the leucogranitic dyke has undergone the D_2 deformation and metamorphism after its emplacement. Zircons extracted from this sample are typically euhedral and prismatic in crystal shapes, transparent to light brown in color, and vary from 50 μm to 200 μm in grain size. CL images show that zircons have oscillatory zoning with high

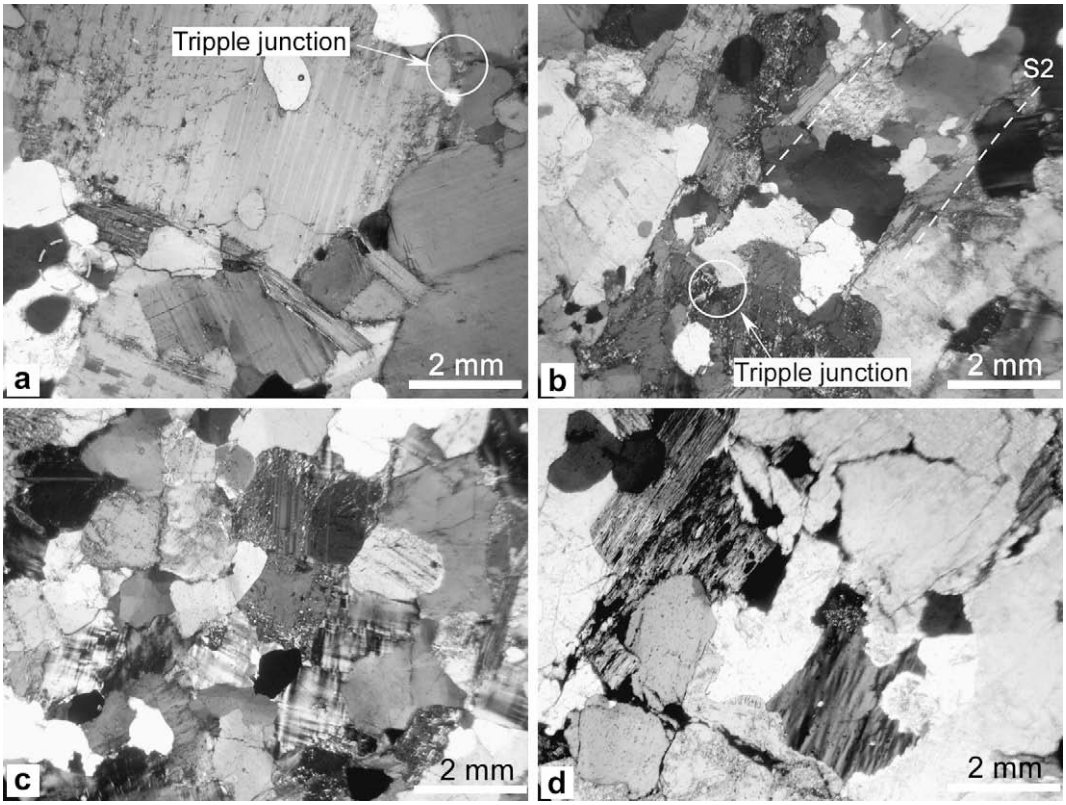

Fig. 11. Photomicrographs for the syn-tectonic leucocratic dykes. (a) Sample FP085-1 shows a blastogranitic texture in which large, tabular igneous plagioclases exist with small subhedral quartz, plagioclase and K-fieldspar grains with triple-junction textures. (b) Sample FP077-2 shows an orientated gneissic foliation. K-feldspar occurs as elongate (length-to-width ratio of 2:1) anhedral crystals parallel to the biotite foliation. In local places, K-feldspar, plagioclase and quartz grains form a triple-junction texture. (c) Sample FP077-3 shows typically magmatic texture, with equigranular K-feldspar, plagioclase and quartz grains. Quartz shows a slight undulose extincition, indicating a gentle post-crystalline deformation (d) Sample FP052-2 shows coarse-grained magmatic texture with weakly orientated foliation.

luminescent inner zones and faded outer zones (Fig. 12d, e), indicating a magmatic origin. The U and Th contents of the zircons range from 553 to 4497 ppm and 89 to 6604 ppm, respectively, with Th/U rations of 0.08–1.52 (Table 2). On a Concordia diagram, thirteen analytical data define a discordant line with an upper intercept age at 1844 ± 18 Ma (MSWD = 4.8; Fig. 13b), interpreted as the approximate crystallization age of this deformed leucogranitic dyke, which is consistent with the age of sample FP085-1.

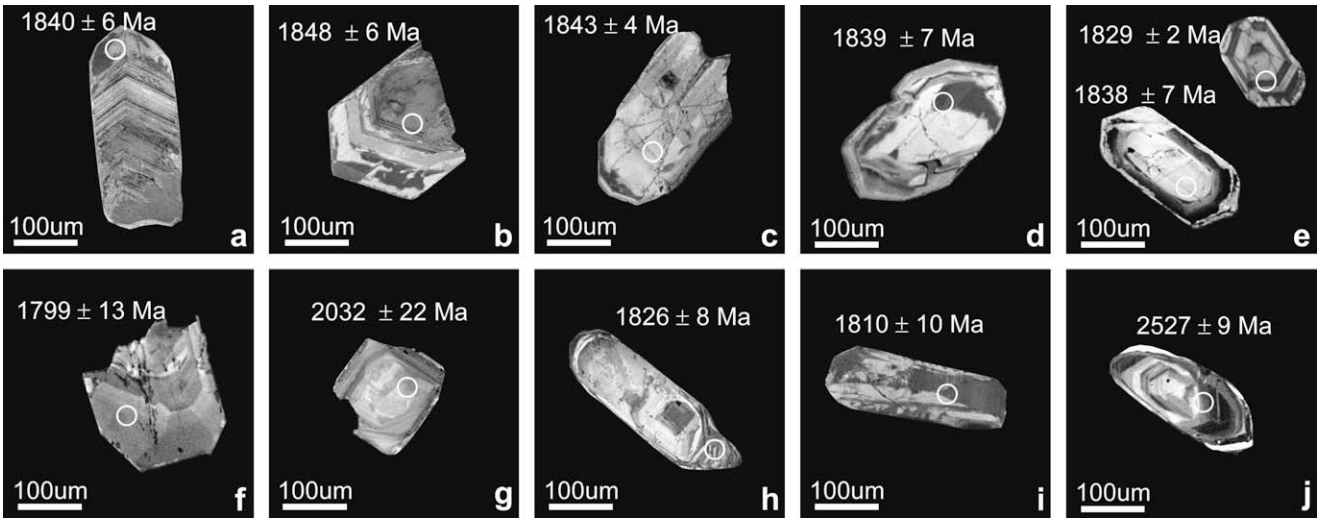

Fig. 12. Representative selection of cathodeluminescence (CL) zircon images with SHRIMP zircon U–Pb dating results from the syn-tectonic leucocratic dykes. (a) A euhedral and prismatic zircon grain with inner concentric oscillatory zoning and outer nebulous zoning (sample FP085-1). (b) A euhedral zircon with blurred patchy zoning (sample 085-1). (c) A subhedral zircon grain with patchy internal zoning (sample FP085-1). (d) A subhedral zircon grain with patchy internal zoning (sample FP077-2). (e) Two prismatic euhedral zircons with sharp terminations and oscillatory zoning (sample FP077-2). (f) An anhedral zircon grain with oscillatory internal zoning (sample FP077-3). (g) A xenocrystic zircon with sharp terminations and concentric oscillatory zoning (sample FP077-3). (h) A subhedral and elongated zircon grain with oscillatory zoning (sample FP052-2). (i) A long prismatic zircon with blurred patchy CL image (sample FP052-2). (j) A xenocrystic zircon with a concentric oscillatory zoned core and a highly luminescent and structureless metamorphic rim (sample FP052-2).

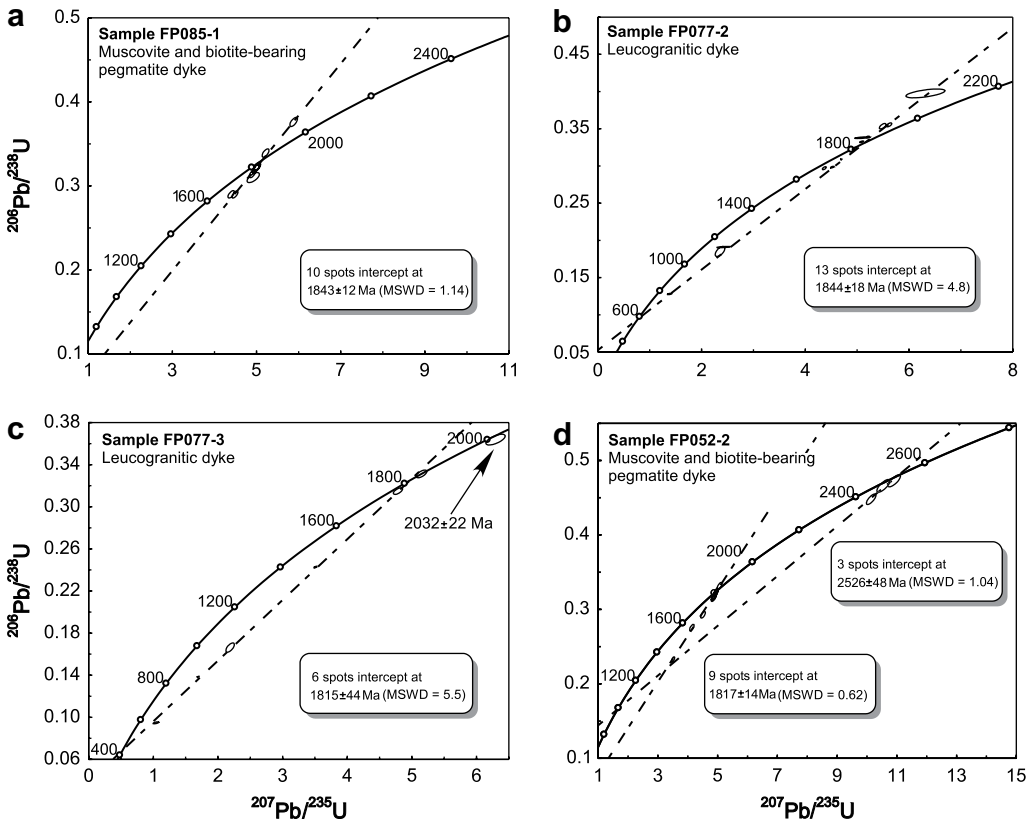

Fig. 13. Concordia diagrams of SHRIMP U–Pb zircon analytical result for samples (a) FP085-1. (b) FP077-2. (c) FP077-3. (d) FP052-2.

Like sample 077-2, FP077-3 is also composed of fine-grained K-feldspar (40%), plagioclase (30%), quartz (15%), biotite (10%) and muscovite (5%), but shows a massive structure (Fig. 11c). The texture is typically magmatic, with equigranular K-feldspar, plagioclase and quartz grains. Quartz shows a slight undulose extincition, indicating a gentle post-crystalline deformation (Fig. 11c). Zircons from this sample are prismatic, transparent and euhedral. CL images show that most zircons possess concentric oscillatory zoning (Fig. 12f), indicative of magmatic origin. The Th and U contents of the zircons are considerably variable from 49 to 5670 ppm and 4 to 9570 ppm, respectively, with Th/U ratios of 0.03–1.74 (Table 2). On a Concordia diagram (Fig. 13c), of seven analyses made on seven zircon grains, six data-points are discordant and define a line with an upper intercept age at 1815 ± 44 Ma

Table 1
U–Th–Pb SHRIMP data (with 1σ errors) for samples FP085-1 and FP052-2.

Sample no.	U (ppm)	Th (ppm)	Th/U	% comm ^{206}Pb	^{207}Pb/^{206}Pb	% Error	^{206}Pb/^{238}U	% Error	^{207}Pb/^{235}U	% Error	^{206}Pb/^{238}U Age ± 1σ (Ma)	^{207}Pb/^{235}U Age ± 1σ (Ma)	^{207}Pb/^{206}Pb Age ± 1σ (Ma)
085-1-1.1	568	13	0.02	0.08	0.1115	0.33	0.3383	0.96	5.20	1.02	1878 ± 16	1852 ± 9	1823 ± 6
085-1-2.1	517	15	0.03	0.07	0.1130	0.33	0.3132	0.97	4.88	1.02	1757 ± 15	1799 ± 9	1848 ± 6
085-1-3.1	959	27	0.03	0.01	0.1127	0.23	0.3207	0.99	4.98	1.01	1793 ± 15	1817 ± 9	1843 ± 4
085-1-4.1	947	12	0.01	0.25	0.1153	1.42	0.3088	1.32	4.91	1.93	1735 ± 20	1804 ± 16	1884 ± 26
085-1-5.1	507	7	0.01	0.01	0.1130	0.32	0.3213	0.97	5.01	1.02	1796 ± 15	1820 ± 9	1848 ± 6
085-1-6.1	325	5	0.02	0.07	0.1127	0.43	0.3192	0.99	4.96	1.08	1786 ± 15	1813 ± 9	1844 ± 8
085-1-7.1	579	13	0.02	0.07	0.1132	0.30	0.3757	0.96	5.87	1.01	2056 ± 17	1956 ± 9	1852 ± 5
085-1-8.1	338	5	0.02	0.06	0.1100	0.77	0.2886	0.99	4.38	1.26	1635 ± 14	1708 ± 10	1800 ± 14
085-1-9.1	733	14	0.02	0.14	0.1124	0.32	0.2885	0.96	4.47	1.01	1634 ± 14	1726 ± 8	1838 ± 6
085-1-10.1	536	9	0.02	0.07	0.1125	0.33	0.3226	0.97	5.00	1.02	1802 ± 15	1820 ± 9	1840 ± 6
052-2-1.1	476	154	0.33	0.24	0.1116	0.44	0.3141	0.97	4.834	1.07	1761 ± 15	1791 ± 9	1826 ± 8
052-2-2.1	513	292	0.59	0.00	0.1115	0.32	0.3156	0.97	4.850	1.02	1768 ± 15	1794 ± 9	1823 ± 6
052-2-3.1	376	151	0.42	−0.01	0.1109	0.38	0.3212	0.98	4.913	1.05	1796 ± 15	1805 ± 9	1815 ± 7
052-2-4.1	382	153	0.42	−0.02	0.1110	0.38	0.3181	0.98	4.868	1.05	1781 ± 15	1797 ± 9	1816 ± 7
052-2-5.1	447	254	0.59	0.36	0.1086	0.46	0.2742	0.97	4.106	1.08	1562 ± 13	1655 ± 9	1776 ± 8
052-2-6.1	446	21	0.05	0.05	0.1113	0.55	0.2913	0.98	4.472	1.12	1648 ± 14	1726 ± 9	1821 ± 10
052-2-7.1	663	212	0.33	0.02	0.1107	0.29	0.3222	0.96	4.915	1.00	1800 ± 15	1805 ± 8	1810 ± 5
052-2-8.1	258	79	0.32	−0.01	0.1637	0.35	0.4469	1.01	10.088	1.07	2381 ± 20	2443 ± 10	2494 ± 6
052-2-9.1	701	225	0.33	0.15	0.1089	0.38	0.2313	0.96	3.474	1.03	1341 ± 12	1521 ± 8	1782 ± 7
052-2-10.1	107	57	0.56	0.05	0.1669	0.53	0.4716	1.13	10.851	1.25	2491 ± 23	2510 ± 12	2527 ± 9
052-2-11.1	76	53	0.72	0.08	0.1638	0.66	0.4647	1.19	10.497	1.37	2460 ± 24	2480 ± 13	2496 ± 11
052-2-12.1	487	179	0.38	0.02	0.1106	0.37	0.3295	0.98	5.022	1.05	1836 ± 16	1823 ± 9	1809 ± 7

Table 2
U–Th–Pb SHRIMP data (with 1σ errors) for samples FP077-2 and FP077-3.

Sample no.	U (ppm)	Th (ppm)	Th/U	% comm ^{206}Pb	$^{207}Pb/^{206}Pb$	% Error	$^{206}Pb/^{238}U$	% Error	$^{207}Pb/^{235}U$	% Error	$^{206}Pb/^{238}U$ Age ± 1σ (Ma)	$^{207}Pb/^{235}U$ Age ± 1σ (Ma)	$^{207}Pb/^{206}Pb$ Age ± 1σ (Ma)
077-2-1.1	1476	1171	0.82	0.69	0.1114	0.36	0.2950	0.23	4.5286	0.43	1666 ± 3	1736 ± 4	1822 ± 7
077-2-2.1	553	166	0.31	0.13	0.1124	0.41	0.3198	0.36	4.9571	0.54	1789 ± 6	1812 ± 5	1839 ± 7
077-2-3.1	1782	1380	0.80	0.50	0.0948	0.45	0.1813	2.50	2.3709	2.54	1074 ± 25	1234 ± 18	1525 ± 9
077-2-4.1	4335	4174	0.99	0.24	0.0819	1.86	0.1243	0.54	1.4040	1.94	755 ± 4	891 ± 12	1243 ± 37
077-2-5.1	1849	2311	1.29	0.46	0.0943	3.41	0.1873	0.31	2.4347	3.42	1107 ± 3	1253 ± 25	1513 ± 64
077-2-6.1	1029	146	0.15	0.30	0.1163	3.78	0.3940	0.98	6.3199	3.90	2141 ± 18	2021 ± 35	1901 ± 68
077-2-7.1	2220	1119	0.52	0.34	0.1109	1.84	0.3344	0.23	5.1115	1.86	1860 ± 4	1838 ± 16	1814 ± 33
077-2-8.1	3385	4643	1.42	0.01	0.1118	0.13	0.3052	0.11	4.7033	0.17	1717 ± 2	1768 ± 1	1829 ± 2
077-2-9.1	1973	1334	0.70	0.07	0.1127	0.16	0.3356	0.18	5.2133	0.24	1865 ± 3	1855 ± 2	1843 ± 3
077-2-10.1	4497	6604	1.52	0.06	0.1123	0.40	0.3289	0.19	5.0953	0.44	1833 ± 3	1835 ± 4	1838 ± 7
077-2-11.1	1221	89	0.08	0.33	0.1139	0.42	0.3499	0.65	5.4954	0.77	1934 ± 11	1900 ± 7	1863 ± 8
077-2-12.1	2088	398	0.20	0.29	0.1080	0.32	0.2936	0.47	4.3728	0.57	1659 ± 7	1707 ± 5	1766 ± 6
077-2-13.1	2105	987	0.48	0.23	0.1160	0.27	0.3515	0.51	5.6206	0.57	1942 ± 9	1919 ± 5	1895 ± 5
077-3-1.1	5670	9570	1.74	1.57	0.0798	3.02	0.0926	0.6	1.02	3.08	571 ± 3	714 ± 16	1193 ± 60
077-3-2.1	142	4	0.03	0.06	0.1125	0.77	0.3313	0.7	5.14	1.06	1845 ± 12	1842 ± 9	1840 ± 14
077-3-3.1	5536	8730	1.63	0.21	0.0953	0.81	0.1648	1.8	2.17	1.99	983 ± 17	1170 ± 14	1535 ± 15
077-3-4.1	180	149	0.86	0.05	0.1100	0.74	0.3147	0.7	4.77	0.99	1764 ± 10	1780 ± 8	1799 ± 13
077-3-5.1	49	30	0.64	0.22	0.1252	1.26	0.3642	0.9	6.29	1.57	2002 ± 16	2017 ± 14	2032 ± 22
077-3-6.1	3289	4064	1.28	1.30	0.0886	0.61	0.1369	0.2	1.67	0.63	827 ± 1	998 ± 4	1396 ± 12
077-3-7.1	1147	795	0.72	0.07	0.1048	0.38	0.2420	0.2	3.50	0.44	1397 ± 3	1526 ± 3	1710 ± 7

(MSWD = 5.5), interpreted to approximate the crystallization age of the undeformed leucogranitic dyke. One data-point (077-3-5.1; Table 2) analyzed on one prismatic zircon (Fig. 12g) is concordant and gives a much older apparent $^{206}Pb/^{207}Pb$ age of 2032 ± 22 Ma (Fig. 13c), which is remarkably similar to the age of the Nanying monzogranitic gneiss (Zhao et al., 2002) and thus is interpreted as the age of a xenocrystic zircon captured from the Nanying gneiss.

4.2.3. Sample FP052-2

Sample FP052-2 was collected from a muscovite–biotite-bearing pegmatite dyke in the 10 km northwest to the Tuanpokou Village (lat. N38°40.972′; long. E113°53.217′) (Fig. 3). The host TTG gneiss has pervasively undergone intense deformation and migmatization to form stromatic migmatites. The leucosomes in stromatic migmatites are parallel or sub-parallel to the fabric of the host gneisses, indicating an in-situ melting or segregation of the gneisses. The pegmatite dyke displays structures similar to those of migmatite leucosomes (Fig. 10c). The pegmatite dyke cuts the S_2 foliation of the host gneisses, but the margin of the dyke shows weak deformational fabrics obliquely truncating the foliation (S_1// S_2) of the host gneisses. In some places, such pegmatite dykes exhibit upright open F_3 folds. The pegmatite consists of coarse-grained K-feldspar (75%), quartz (15%), and biotite (10%), of which the latter shows a weak preferred orientation (Fig. 11d). All these features suggest that the pegmatite dyke could have formed after the D_2 deformation and earlier than the D_3 deformation, and thus its age can be used to approximately constrain the timing of the D_2 and D_3 deformation.

Two groups of morphologically different zircons were recognized from the sample. Group I consists of translucent to turbid, 300–600 μm prismatic zircon grains. Most grains are too dark for CL image studying, whereas some zircons show blurred and patchy zoning in CL images (Fig. 12h, i). This feature suggests that the zircons are magmatic origin although they may have suffered alteration in the presence of hydrothermal fluid. Group II are fine-grained (<200 μm), totally transparent, oval zircon grains, with typical oscillatory zoning, suggesting an igneous origin (Fig. 12j). Some of these grains have high luminescent, structureless and narrow rims that are too thin to be measured by SHRIMP and presumably reflect metamorphic overgrowth (Fig. 12j). A total of twelve analyses were taken on twelve zircon grains, of which nine analytical data-points were from the zircons of Group I and three from Group II. U and Th contents of all the zircons range between 76 and 701 ppm and between 21 and 292 ppm, respectively, and the Th/U ratio ranges between 0.05 and 0.72 (Table 1). On a Concordia diagram (Fig. 13d), the analytical measurements define two discordant populations. One population constituted by nine spots from Group I defines an upper discordant intercept age of 1817 ± 14 Ma (MSWD = 0.62) (Fig. 13d), interpreted as the approximate crystallization age of the pegmatite dyke. The other population of three data-points of the Group II zircons defines an upper discordant intercept age of 2526 ± 48 Ma (MSWD = 1.04) (Fig. 13d), which is bracketed to the age range (2523–2486 Ma) of the Fuping TTG gneiss (Guan et al., 2002; Zhao et al., 2002), suggesting that they are xenocrystic zircons from the TTG gneiss.

5. Discussion

5.1. Structural summary

D_1 resulted in the formation of isoclinal folds F_1 and penetrative foliations S_1. The preserved L_1 mineral stretching lineations indicate an earlier NW–SE-oriented thrusting or shearing (Fig. 14b).

D_2 is the major stage of deformation that progressively overprinted the D_1 fabrics and generated variable scales of the tight to isoclinal F_2 folds and penetrative S_2 foliations. D_2 also resulted in the development of regional-scale ductile shear zones (e.g. the Longquanguan ductile shear zone). Our structural data show that the Longquanguan ductile shear zone has similar structural features with the D_2 structures of the other Fuping lithologies, suggesting that it developed during D_2, not the consequence of the D_1 deformation as Trap et al. (2007) suggested. Both of the D_2 thrust faults and syn-D_2 kinematic indicators indicate a top-to-the-SE(E) sense of thrusting, and are interpreted to have resulted from the progressive shortening during the collision, causing the crustal thickening and the peak metamorphism (M_1) (Fig. 14b).

D_3 is characterized by open meso-scale folds, refolding the D_1 and D_2 fabrics to be dome-and-basin interference patterns. Unlike the ductile D_1 and D_2 stages of deformation, the D_3 deformation generated semi-ductile to brittle fabrics (Fig. 9e) and occurred during the exhumation or uplift after the crustal thickening (Fig. 14c). During D_3, the Fuping lithologies underwent rapid

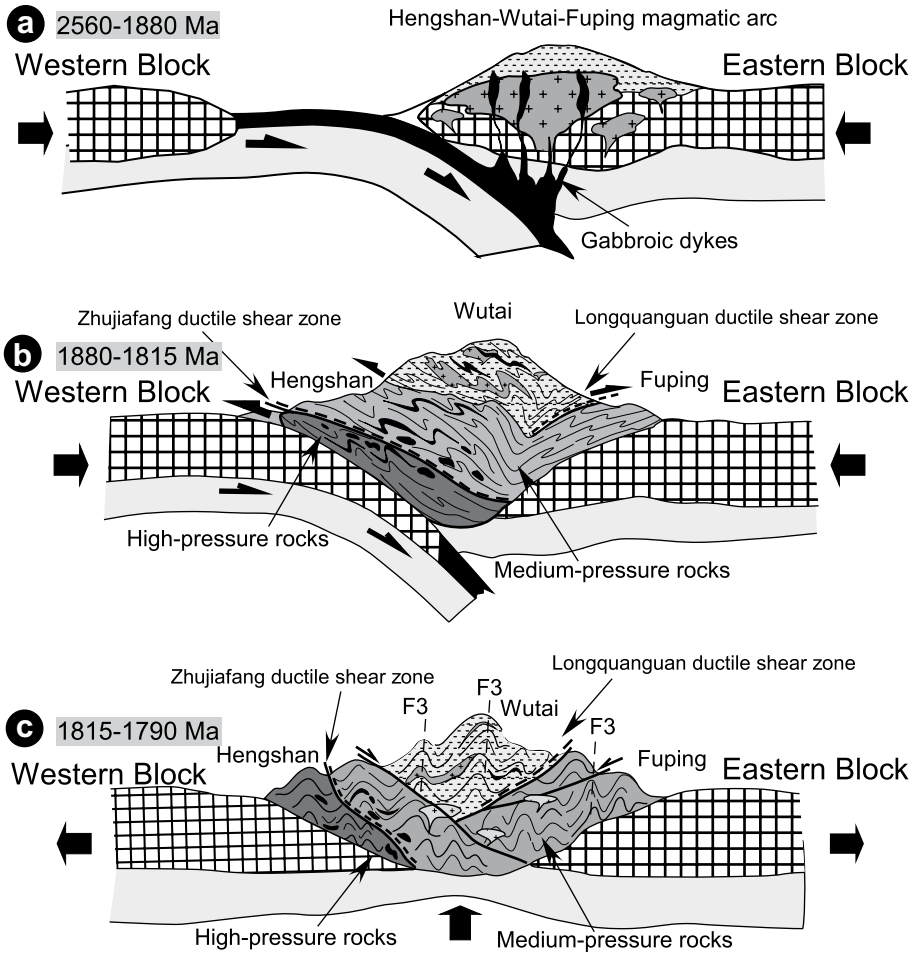

Fig. 14. Tectonic scenario for the evolution of the Hengshan–Wutai–Fuping mountain belt and the TNCO (modified after Zhang et al., 2007). (a) At 2650–1880 Ma, the Hengshan, Wutai and Fuping Complexes were part of a magmatic arc that developed under an eastward subduction between the Western and Eastern Blocks. (b) At 1880–1815 Ma, continent–arc–continent collision between the two blocks led to crustal-scale deformation (D_1 and D_2) and the formation of the fan-shaped orogenic wedge, generating top-to-the-NW thrusting and shearing structures with high-pressure granulite-facies metamorphism in the forearc (Hengshan), and resulting in the back folding and thrusting in the hinterland (Fuping) with medium-pressure granulite-facies metamorphism. (c) At 1815–1800 Ma, post-collisonal extension (D_3) resulted in the isostatic exhumation of the deeper-seated high-grade rocks, ductile to brittle structures in different crustal levels and pervasively decompressional metamorphism of the orogen.

exhumation that was associated with widespread decompression metamorphism (M_2), represented by the development of orthopyroxene + plagioclase symplectites in the mafic granulites (Zhao et al., 2000b). Finally, the Fuping Complex was exhumed to the shallow crustal levels where all the lithologies experienced cooling and retrogressive metamorphism (M_3) to form hornblende + plagioclase symplectites in the mafic granulites.

In summary, the three stages (D_1, D_2 and D_3) of deformation in the Fuping Complex record progressive tectonic processes characterized by the initial thrusting and crustal thickening followed by subsequent exhumation/uplift, which is consistent with the continent–continent collision between the Eastern and Western Blocks to form the North China Craton (Fig. 14).

5.2. Constraints on the timing of collision between the Eastern and Western Blocks

There are no direct geochronological constraints on the absolute timing of the D_1 deformation. Recent SHRIMP U–Pb zircon dating on metamorphic zircons and electron probe microanalysis (EPMA) on monazites suggest that the metamorphism of the Fuping Complex and other complexes in the TNCO occurred at 1880–1820 Ma (Guan et al., 2002; Zhao et al., 2002; Kröner et al., 2005a,b, 2006; Liu et al., 2006; Faure et al., 2007; Trap et al., 2007), which has been considered to result from the collision between the Eastern and Western Blocks. Therefore, the D_1 deformation most likely occurred slightly earlier or synchronously at ca. 1880 Ma.

Based on the structural studies, the earliest collision triggered the D_1 deformation to produce a regional penetrative foliation (S_1). Progressive compression led to the development of the overturned to recumbent F_2 folds that overprinted the earlier D_1 fabrics. One such structure is illustrated by the pegmatite sample FP085-1. This pegmatite dyke shows an asymmetric fold (F_2) with very clear sequence of pegmatite intrusion enclosing the deformed TTG gneiss as xenoliths (Fig. 10a). Magmatic zircons from the pegmatite dyke yielded a SHRIMP U–Pb age of 1843 ± 12 Ma, indicating that D_1 must have taken place at some time before 1843 ± 12 Ma, whereas D_2 happened at some time after 1843 ± 12 Ma. In addition, a leucogranitic dyke (sample FP077-2) that has deformational structures similar to those of sample FP085-1 (Fig. 10b) yields a SHRIMP U–Pb age of 1844 ± 18 Ma, suggesting that it was also emplaced after the D_1 deformation and underwent the subsequent D_2 deformation. As mentioned above, the D_1 and D_2 stages of deformation have intimate successive relationships in the field. Hence, we can infer that the D_1 deformation could have occurred at some time shortly before 1843 Ma. This is consistent with our inference that the D_1 deformation could have occurred at ca. 1880 Ma. Generally metamorphism is interpreted to have been synchronous with, and to have been slightly after the major D_2 deformation, regardless of when D_2 developed or was reworked

(e.g. Gibson et al., 2005). Therefore, the ages of 1843 ± 12 Ma and 1844 ± 18 Ma are in accord with the timing of metamorphism (1875–1802 Ma) in the Fuping Complex (Guan et al., 2002; Zhao et al., 2002). After the D_2 deformation, the D_3 deformation characterized by open folds (F_3) did not markedly produce penetrative fabrics and only slightly reworked the earlier structures. One leucocratic dyke (sample FP052-2) has weakly deformed fabrics that obliquely truncate the host S_2 foliations (Fig. 10c), indicating that it most probably formed after the D_2 deformation and underwent the D_3 deformation. It yielded the SHRIMP U–Pb zircon age of 1817 ± 14 Ma, suggesting that D_2 must have occurred at some time earlier than this age, but D_3 must have taken place at some time later than 1817 ± 14 Ma. A similar SHRIMP U–Pb zircon age of 1815 ± 44 Ma was obtained from a coarse-grained and weakly deformed leucogranitic dyke (sample FP077-3). After the orogenesis, the Fuping Complex was exhumed to a shallow crustal level in which the complex underwent retrogression and post-collisional extension, which was associated with the emplacement of undeformed granitic pegmatites and mafic dykes that were previously dated at 1779–1790 Ma (Wilde et al., 1998; Liu et al., 2000; Wang et al., 2003). New SHRIMP U–Pb zircon ages for the deformed leucocratic dykes suggest that the major deformation of the Fuping Complex may have occurred at ~1850 Ma, indicative of the timing of collision between the Eastern and Western Blocks.

5.3. Subduction polarity

A major debate on the tectonic evolution of the TNCO is the subduction polarity of the oceanic lithosphere between the Eastern and Western Blocks of the North China Craton, with some researchers proposing a westward subduction (Kusky et al., 2001, 2007; Kusky and Li, 2003; Polat et al., 2005; Li and Kusky, 2007; Faure et al., 2007; Trap et al., 2007) and others arguing for an eastward subduction (Wu and Zhong, 1998; Zhao, 2001; Zhao et al., 1998, 1999, 2000a, 2001a, 2007; Wilde et al., 2002; Kröner et al., 2005a,b, 2006; Zhang et al., 2007). Current available data are insufficient to resolve this controversial issue, but structural data presented in this study, combined with metamorphic and geochemical data, can provide some constraints on it. Our structural data indicate that the Fuping Complex is characterized by a series of SE(E)-verging overturned to recumbent folds and top-to-the-SE(E) thrusts, which were also recognized by other researchers and considered to be related to either the forearc thrusts (Fig. 2b; Polat et al., 2005; Kusky and Li, 2003; Li and Kusky, 2007) or intracontinental thrusts (Fig. 2c; Faure et al., 2007; Trap et al., 2007) involved in the westward subduction. However, an orogenic belt normally shows different structural patterns and thrusting senses in different positions (e.g. the Himalayas, Ziegler et al., 1995, 1998; the Alps, Escher and Beaumont, 1997; TRANSALP, 2002; Castellarin et al., 2006; Lüschen et al., 2006; the Appalachians, Lin et al., 1994; Castonguay and Tremblay, 2003). This is the case with the TNCO, where the Fuping, Wutai and Hengshan Complexes constitute a representative cross-section in its central segment but exhibit different structural patterns and thrusting senses. Our recent studies have revealed that the structures of the Hengshan Complex are different from that of the Fuping Complex (Zhang et al., 2007). The former is characterized by moderate-to-high dipping foliations and top-to-the-NW thrusts (Fig. 14b; Zhang et al., 2007), whereas the latter is represented by shallow dipping foliations and top-to-the-SE(E) thrusts. The intervened Wutai Complex has similar structural features to those of the Hengshan Complex in its northwestern part and to those of the Fuping Complex in its southeastern part (Tian, 1991; Zhang et al., unpublished data). The structural pattern of the Hengshan–Wutai–Fuping mountain belt generally represents a fan-shaped orogenic wedge transecting the TNCO (Fig. 14b). Theoretically, such structural patterns and opposite thrusting senses from Hengshan, through Wutai, to Fuping may be explained by both the westward- and eastward subduction models. However, an integrated synthesis of the following geological data combined with structural data of this study favors the eastward subduction model:

(1) Recent geological and geochemical data show that the TNCO was originally an Andean-type continental margin arc or a Japan-type island arc (Zhao et al., 2005, 2007; Liu et al., 2002, 2004, 2005; Wang et al., 2004b; Kröner et al., 2005a,b, 2006), with the earliest arc-related magmatism occurring at 2560–2520 Ma, represented by the emplacement of the Wutai granitoids. Recent SHRIMP U–Pb zircon data revealed the existence of 2.65–2.85 Ga old continental remnants in the arc-related granitoids and volcanic rocks of the TNCO (Liu et al., 1997; Wilde et al., 1997, 2004; Zhao et al., 2002; Guan et al., 2002; Kröner et al., 2005a,b). The 2.65–2.85 Ga rocks are widely distributed in the western part of the Eastern Block (e.g. Western Shandong, Jahn et al., 1988). In contrast, available data show that few rocks in the Western Block are older than 2.6 Ga (Xia et al., 2006a). Hf and Nd isotopic data also show that the rocks of the TNCO have affinities to those of the Eastern Blocks, but are in contrast with that of the Western Block (Xia et al., in press). This provides strong evidence that the magmatic arc of the TNCO developed on the western margin of the Eastern Block. The subduction of the oceanic lithosphere between the Western and Eastern Blocks must have been initially eastward-directed (Fig. 14a).
(2) High-pressure granulites and retrograded eclogites are only exposed in the Hengshan Complex along the western margin of the TNCO (Zhao et al., 2001b; Kröner et al., 2005a, 2006; O'Brien et al., 2005). Generally, high-pressure metamorphism of an orogenic belt can take place either in rocks that are part of the downgoing slab or in material that has been accreted to the base of the overlying plate (Miyashiro et al., 1979). In any case, however, high-pressure rocks in an orogenic belt generally occur close to the subducted slab or the trench (Miyashiro et al., 1979). In this case, the Hengshan Complex was most possibly located in the area close to the subducted slab, whereas the Fuping Complex was far from the subducted slab during the collision (Fig. 14b).

6. Conclusions

Major conclusions from the above structural and geochronological data for the Fuping Complex in the TNCO are summarized as follows:

(1) The Fuping Complex in the TNCO underwent three stages of deformation (D_1, D_2 and D_3). The D_1 deformation recorded the early NW–SE-orientated collision. The subsequent D_2 deformation successively overprinted the D_1 deformation and produced E to SE-verging overturned to recumbent folds and thrusting faults of variable scales. D_1 and D_2 resulted in the crustal shortening and thickening, and are responsible for the peak metamorphism. The D_3 deformation produced semi-ductile to brittle structures and was responsible for the exhumation and decompressional metamorphism of the whole complex. The three stages (D_1, D_2 and D_3) of deformation in the Fuping Complex record progressive tectonic processes characterized by the initial thrusting and crustal thickening followed by subsequent exhumation/uplift, which has also been inferred from metamorphic studies (Liu and Liang, 1997; Zhao et al., 2000b).
(2) SHRIMP U–Pb ages of several phases of leucocratic dykes have been used to approximately define the timing of different

deformational stages. Two leucocratic dykes emplaced at a time between D_1 and D_2 yield SHRIMP zircon ages of 1843 ± 12 Ma and 1844 ± 18 Ma, which indicate that D_1 must have occurred at some time earlier than ~1844 Ma, whereas D_2 must have occurred at some time later than this age. Two post-D_2 leucocratic dykes give SHRIMP zircon ages of 1815 ± 45 Ma and 1817 ± 14 Ma. Thus, the timing of the D_2 deformation was restricted between 1843 and 1815 Ma. Considering the previously published zircon age of 1799 ± 9 Ma for a post-tectonic undeformed granitic pegmatite dyke of the complex, the D_3 deformation should have occurred between 1817 and 1800 Ma. The SHRIMP zircon ages of these leucocratic dykes confirm that the deformational episodes of the Fuping Complex occurred in the late Paleoproterozoic, not at the end of the late Archean as previously considered.

(3) The difference of structural patterns in the Fuping Complex and the adjacent Hengshan and Wutai Complexes indicate that they may represent different tectonic positions transecting the TNCO. Considering the presence of high-pressure granulites and retrograded eclogites in the Hengshan Complex and the remnants of a continental crust represented by minor 2.8–2.6 Ga rocks and zircons in the TNCO, we suggest that the Hengshan Complex was situated in the area closer to the subducted slab than the Fuping Complex. Thus, the combination of structural, metamorphic and geochronological data for the Hengshan–Wutai–Fuping region favors an eastward subduction model for the evolution of the TNCO, though the final determination of the subduction polarity of the TNCO needs further extensive geological investigations through the whole orogen.

Acknowledgements

This research was financially supported by an NSFC Outstanding Overseas Young Researcher Grant (40429001), and the 111 Project (No. B07011) from the Ministry of Education of China, and Hong Kong RGC grants (HKU7063/06P, 7055/05P, 7058/04P and 7049/04P). We thank Jianbo Zhou for his kind assistance in SHRIMP dating at Curtin University of Technology (Western Australia) and Wenlue Shen for his constructive discussions. The final version of the paper has benefited from the perceptive and critical comments of Wenjiao Xiao and an anonymous reviewer and Journal Editor T.G. Blenkinsop.

References

Bai, J., 1986. The Precambrian crustal evolution of the Wutaishan area. In: Bai, J. (Ed.), The Early Precambrian Geology of Wutaishan. Tianjin Science and Technology Press, Tianjin, pp. 376–383 (in Chinese).

Castellarin, A., Nicolich, R., Fantoni, R., Cantelli, L., Sella, M., Selli, L., 2006. Structure of the lithosphere beneath the Eastern Alps (southern sector of the TRANSALP transect). Tectonophysics 414, 259–282.

Castonguay, S., Tremblay, A., 2003. Tectonic evolution and significance of Silurian – early Dvonian hinterland-directed deformation in the internal Humber zone of the southern Quebec Appalachians. Canadian Journal of Earth Sciences 40, 255–268.

Escher, A., Beaumont, C., 1997. Formation, burial and exhumation of basement nappes at crustal scale: a geometric model based on the Western Swiss–Italian Alps. Journal of Structural Geology 19, 955–974.

Faure, M., Trap, P., Lin, W., Monie, P., Bruguier, O., 2007. Polyorogenic evolution of the Paleoproterozoic Trans-North China Belt, new insights from the Lüliangshan–Hengshan–Wutaishan and Fuping massifs. Episodes 30, 1–12.

Gibson, H.D., Brown, R.L., Carr, S.D., 2005. U–Th–Pb geochronologic constraints on the structural evolution of the Selkirk fan, northern Selkirk Mountains, southern Canadian Cordillera. Journal of Structural Geology 27, 1899–1924.

Guan, H., Sun, M., Wilde, S.A., Zhou, X.H., Zhai, M.G., 2002. SHRIMP U–Pb zircon geochronology of the Fuping Complex: implications for formation and assembly of the North China Craton. Precambrian Research 113, 1–18.

Guo, J.H., O'Brein, P.J., Zhai, M.G., 2002. High-pressure granulites in the Sangan area, North China Craton: metamorphic evolution, P–T paths and geotectonic significance. Journal of Metamorphic Geology 20, 741–756.

Guo, J.H., Sun, M., Zhai, M.G., 2005. Sm–Nd and SHRIMP U–Pb Zircon geochronology of high-pressure granulites in the Sangan area, North China Craton: timing of Palaeoproterozoic continental collision. Journal of Asian Earth Sciences 24, 629–642.

Hao, D.F., Li, S.Z., Zhao, G.C., Sun, M., Han, Z.Z., Zhao, G.T., 2004. Origin and its constraint to tectonic evolution of Paleoproterozoic granitoids in the eastern Liaoning and Jilin provinces, North China. Acta Petrologica Sinica 20 (6), 1409–1416 (in Chinese with English abstract).

Jahn, B.M., Auvray, B., Shen, Q.H., Liu, D.Y., Zhang, Z.Q., Dong, Y.J., Ye, X.J., Cornichet, J., Mace, J., 1988. Archean crustal evolution in China: the Taishan Complex and evidence from Juvenile crustal addition from long-term depleted mantle. Precambrian Research 38, 381–403.

Kröner, A., Wilde, S.A., Li, J.H., Wang, K.Y., 2005a. Age and evolution of a late Archaean to early Palaeozoic upper to lower crustal section in the Wutaishan/Hengshan/Fuping terrain of northern China. In: Wilde, S.A., Zhao, G.C. (Eds.), Late Archean to Paleoproterozoic Evolution of the North China Craton. Journal of Asian Earth Sciences 24, 577–595.

Kröner, A., Wilde, S.A., O'Brein, P.J., Li, J.H., Passchier, C.W., Walte, N.P., Liu, D.Y., 2005b. Field relationships, geochemistry, Zircon ages and evolution of a late Archean to palaeoproterozoic lower crustal section in the Hengshan terrain of Northern China. Acta Geologica Sinica 79, 605–629.

Kröner, A., Wilde, S.A., Zhao, G.C., O'Brein, P.J., Sun, M., Liu, D.Y., Wan, Y.S., Liu, S.W., Guo, J.H., 2006. Zircon geochronology and metamorphic evolution of mafic dykes in the Hengshan Complex of northern China: evidence for late Palaeoproterozoic extension and subsequent high-pressure metamorphism in the North China Craton. Precambrian Research 146, 45–67.

Kusky, T.M., Li, J.H., Tucker, R.D., 2001. The Archean Dongwanzi ophiolite complex, North China Craton: 2. 505-billion-year-old oceanic crust and mantle. Science 292, 1142–1145.

Kusky, T.M., Li, J.H., 2003. Paleoproterozoic tectonic evolution of the North China Craton. Journal of Asian Earth Sciences 22, 23–40.

Kusky, T.M., Li, J.H., Santosh, M., 2007. The Paleoproterozoic North Hebei Orogen: North China Craton's collisional suture with the Columbia supercontinent. Gondwana Research 12, 4–28.

Li, J.H., Qian, Q.L., 1991. A study on the Longquanguan shear zone in the northern part of the Taihang Mountains. Shanxi Geology 6, 17–29 (in Chinese).

Li, J.H., Kusky, T.M., 2007. A late Archean foreland fold and thrust belt in the North China Craton: implications for early collisional tectonics. Gondwana Research 12, 47–66.

Li, S.Z., Zhao, G.C., Sun, M., Han, Z.Z., Zhao, G.T., Hao, D.F., 2006. Are the south and North Liaohe Groups of North China different exotic terranes? Nd isotope constraints. Gondwana Research 9, 349–362.

Li, S.Z., Zhao, G.C., 2007. SHRIMP U–Pb zircon geochronology of the Liaoji granitoids: constraints on the evolution of the Paleoproterozoic Jiao-Liao-Ji belt in the Eastern Block of the North China Craton. Precambrian Research 158, 1–16.

Lin, S.F., Lin, S.F., van Staal, C.R., Dube, B., 1994. Promontory–promontory collision in the Canadian Appalachians. Geology 22, 897–900.

Liu, D.Y., Page, R.W., Compston, W., Wu, J.S., 1985. U–Pb zircon geochronology of Late Archean metamorphic rocks in the Taihangshan–Wutaishan area, North China. Precambrian Research 27, 85–109.

Liu, D.Y., Geng, Y.S., Song, B., 1997. Late Archean crustal accretion and reworking in Northwestern Hebei Province: isochronology evidence. Acta Geoscientia Sinica 18, 226–232 (in Chinese with English abstract).

Liu, S.W., Liang, H.H., 1997. Metamorphism of Al-rich gneisses from the Fuping Complex, Taihang Mountain, China. Acta Petrologica Sinica 13, 303–312 (in Chinese with English abstract).

Liu, S.W., Liang, H.H., Hua, Y.G., Jian, A.H., 2000. Isotopic chronology and geological events of Precambrian complex in Taihangshan region. Science in China 43, 386–393.

Liu, S.W., Pan, Y.M., Li, J.H., Zhang, J., Li, Q.G., 2002. Geological and isotopic geochemical constraints on the evolution of the Fuping Complex, North China Craton. Precambrian Research 117, 41–56.

Liu, S.W., Pan, Y.M., Xie, Q.L., Zhang, J., Li, Q.G., 2004. Archean geodynamics in the Central Zone, North China craton: constraints from geochemistry of two contrasting series of granitoids in the Fuping and Wutaishan complexes. Precambrian Research 130, 229–249.

Liu, S.W., Pan, Y.M., Xie, Q.L., Zhang, J., Li, Q.G., 2005. Geochemistry of the Paleoproterozoic Nanying granitoid gneisses: constraints on the tectonic setting of the Central Zone, North China Craton. Journal of Asian Earth Sciences 24, 643–658.

Liu, S.W., Zhao, G.C., Wilde, S.A., Shu, G.M., Sun, M., Li, Q.G., Tian, W., Zhang, J., 2006. Th–U–Pb monazite geochronology of the Lüliang and Wutai Complexes: constraints on the tectonothermal evolution of the Trans-North China Orogen. Precambrian Research 148, 205–224.

Lu, X.P., Wu, F.Y., Guo, J.H., Wilde, S.A., Yang, J.H., Liu, X.M., Zhang, X.O., 2006. Zircon U–Pb geochronological constraints on the Paleoproterozoic crustal evolution of the Eastern block in the North China Craton. Precambrian Research 146, 138–164.

Ludwig, K.R., 2001. Users Manual for a Geochronological Toolkit for Microsoft Excel. In: Special Publication (1a), vol. 59. Berkeley Geochronology Center.

Lüschen, E., Borrini, D., Gebrande, H., Lammerer, B., Millahn, K., Neubauer, F., Nicolich, R., 2006. TRANSALP – deep crustal vibroseis and explosive seismic profiling in the Eastern Alps. Tectonophysics 414, 9–38.

Luo, Y., Sun, M., Zhao, G.C., Li, S.Z., Xu, P., Ye, K., Xia, X.P., 2004. LA–ICP–MS U–Pb zircon ages of the Liaohe Group in the Eastern Block of the North China Craton: constraints on the evolution of the Jiao-Liao-Ji Belt. Precambrian Research 134, 349–371.

Luo, Y., Sun, M., Zhao, G.C., Li, S.Z., Ayers, J.C., Xia, X.P., Zhang, J.H., 2008. A comparison of U–Pb and Hf isotropic compositions of detrital zircons from the North and South Liaohe Groups: constraints on the evolution of the Jiao-Liao-Ji Belt, North China Craton. Precambrian Research 163, 279–306.

Miyashiro, A., Aki, K., Celas Sengor, A.M., 1979. Orogeny. John Wiley, New York.

O'Brien, P.J., Walte, N., Li, J.H., 2005. The petrology of two distinct granulite types in the Hengshan Mts, China, and tectonic implications. Journal of Asian Earth Sciences 24, 615–627.

Pidgeon, R.T., Furfaro, D., Kennedy, A.K., Nemchin, A.A., van Bronswijk, W., Todt, W.A., 1994. Calibration of zircon standards for the Curtin SHRIMP II. Abstracts Eighth International Conference on Geochronology, Cosmochronology and Isotope Geology, Berkeley, 251pp.

Polat, A., Kusky, T., Li, J.H., Fryer, B., Kerrich, R., Patrick, K., 2005. Geochemistry of Neoarchean (ca. 2.55–2.50 Ga) volcanic and ophiolitic rocks in the Wutaishan greenstone belt, central orogenic belt, North China craton: implications for geodynamic setting and continental growth. The Geological Society of America Bulletin 117, 1387–1399.

Polat, A., Herzberg, C., Munker, C., Rodgers, R., Kusky, T.M., Li, J.H., Fryer, B., Delaney, J., 2006. Geochemical and petrological evidence for a supra-subduction zone origin of NeoArchaean (2.55–2.50 Ga) peridotites, central orogenic belt, North China Craton. Geological Society of America Bulletin 118, 771–784.

Santosh, M., Sajeev, K., Li, J.H., 2006. Extreme crustal metamorphism during Columbia supercontinent assembly: evidence from North China Craton. Gondwana Research 10, 256–266.

Santosh, M., Tsunogae, T., Li, J.H., 2007a. Discovery of sapphirine-bearing Mg–Al granulites in the North China Craton: implications for Paleoproterozoic ultrahigh temperature metamorphism. Gondwana Research 11, 263–285.

Santosh, M., Wilde, S.A., Li, J.H., 2007b. Timing of Paleoproterozoic ultrahigh-temperature metamorphism in the North China Craton: evidence from SHRIMP U–Pb zircon geochronology. Precambrian Research 159, 178–196.

Steiger, R.H., Jäger, E.J., 1977. Subcommission on geochronology: convention on the use of decay constants in geo- and cosmochronology. Planetary Science Letters 36, 359–362.

Tian, Y.Q., 1991. Geology and Gold Mineralization of Wutai–Hengshan Greenstone Belt. Shanxi Science and Technology Press, Taiyuan, pp. 1–25 (in Chinese).

TRANSALP Working Group, 2002. First deep seismic reflection images of the Eastern Alps reveal giant crustal wedges and transcrustal ramps. Geophysics Research Letter 29, doi:10.1029/2002GL014911.

Trap, P., Faure, M., Lin, W., Bruguier, O., Monie, P., 2007. Late Paleoproterozoic (1900–1800 Ma) nappe stacking and polyphase deformation in the Hengshan–utaishan area: implications for the understanding of the Trans-North-China Belt, North China Craton. Precambrian Research 156, 85–106.

Wang, Y.J., Fan, W.M., Zhang, Y., Guo, F., 2003. Structural evolution and 40Ar/39Ar dating of the Zanhuang metamorphic domain in the North China Craton: constraints on Paleoproterozoic tectonothermal overprinting. Precambrian Research 122, 159–182.

Wang, Y.J., Fan, W.M., Zhang, Y., Guo, F., 2004a. Geochemical, 40Ar/39Ar geochronological and Sr–Nd isotopic constraints on the origin of Paleoproterozoic mafic dikes from the southern Taihang Mountains and implications for the ca. 1800 Ma event of the North China Craton. Precambrian Research 135, 55–77.

Wang, Z.H., Wilde, S.A., Wang, K.Y., Yu, L.J., 2004b. A MORB-arc basalt–adakite association in the 2.5 Ga Wutai greenstone belt: late Archean magmatism and crustal growth in the North China Craton. Precambrian Research 131, 323–343.

Wilde, S.A., Cawood, P.A., Wang, K.Y., 1997. The relationship and timing of grnitoid evolution with respect to Felsic volcanism in the Wutai Complex, North China Craton. In: Proceedings of the 30th International Geological Congress, Beijing, vol. 17. VSP International Science Publishers, Amsterdam. 75–87.

Wilde, S.A., Cawood, P.A., Wang, K.Y., Nemchin, A., 1998. SHRIMP U–Pb zircon dating of granites and gneisses in the Taihangshan–Wutaishan area: implications for the timing of crustal growth in the North China Craton. Chinese Science Bulletin 43, 144.

Wilde, S.A., Zhao, G.C., Sun, M., 2002. Development of the North China Craton during the Late Archaean and its final amalgamation at 1.8 Ga; some speculations on its position within a global Palaeoproterozoic supercontinent. Gondwana Research 5, 85–94.

Wilde, S.A., Cawood, P.A., Wang, K.Y., Nemchin, A., Zhao, G.C., 2004. Determining Precambrian Crustal evolution in China: a case-study from Wutaishan, Shanxi Province, demonstrating the application of precise SHRIMP U–Pb geochronology. In: Aspects of the Tectonic Evolution of China. Geological Society, London, Special Publications, vol. 226, pp. 5–25.

Wilde, S.A., Zhao, G.C., 2005. Archean to Palaeoproterozoic evolution of the North China Craton. Journal of Asian Earth Sciences 24, 519–522.

Williams, I.S., 1998. U–Th–Pb geochronology by ion microprobe. In: Mckibben, M.A., Shanks III, W.C., Ridley, W.I. (Eds.), Applications of Microanalytical Techniques to Understanding Mineralizing Processes. Reviews in Economic Geology 7, 1–35.

Wu, J.S., Geng, Y.S., Xu, H.F., Jin, L.G., He, S.Y., Sun, S.W., 1989. Metamorphic geology of Fuping Group. Tianjin Institute of Geology Bulletin 19, 1–213 (in Chinese).

Wu, C.H., Zhong, C.T., 1998. The Paleoproterozoic SW–NE collision model for the central North China Craton. Progress in Precambrian Research 21, 28–50 (in Chinese).

Xia, X.P., Sun, M., Zhao, G.C., Wu, F.Y., Xu, P., Zhang, J.H., Luo, Y., 2006a. U–Pb and Hf isotopic study of derital zircons from the Wulashan Khondalites: constraints on the evolution of the Ordos Terrane, Western Block of the North China Craton. Earth and Planetary Science Letters 241, 581–593.

Xia, X.P., Sun, M., Zhao, G.C., Luo, Y., 2006b. LA–ICP–MS U–Pb geochronology of detrital zircons from the Jining Complex, North China Craton and its tectonic significance. Precambrian Research 144, 199–212.

Xia, X.P., Sun, M., Zhao, G.C., Wu, F.Y., Xu, P., Zhang, J., He, Y.H. U–Pb age and Hf isotope study of detrital zircons from Khondalites in the Lüliang Complex and their implications for the origin of the Trans-North China Orogen. Geological Magazine, in press.

Zhang, J., Zhao, G.C., Li, S.Z., Sun, M., Liu, S.W., Wilde, S.A., Kröner, A., Yin, C.Q., 2007. Deformation history of the Hengshan Complex: implications for the tectonic evolution of the Trans-North China Orogen. Journal of Structural Geology 29, 933–949.

Zhang, J.J., Zhao, L., Liu, S.W., 2006. Structures of syn-deformational granites in the Longquanguan Shear Zone and their monazite electronic microprobe dating. Acta Geologica Sinica 80, 864–874.

Zhang, S.G., Jin, L.G., Xiao, Q.H., 1983. Structural style and deformational history of the Fuping Archean domal composite fold group. Regional Geology of China 6, 97–110 (in Chinese with English abstract).

Zhao, G.C., Wilde, S.A., Cawood, P.A., Lu, L.Z., 1998. Thermal evolution of the Archaean basement rocks from the eastern part of the North China Craton and its bearing on tectonic setting. International Geological Review 40, 706–721.

Zhao, G.C., Wilde, S.A., Cawood, P.A., Lu, L.Z., 1999. Tectonothermal history of the basement rocks in the western zone of the North China Craton and its tectonic implications. Tectonophysics 310, 37–53.

Zhao, G.C., Cawood, P.A., Wilde, S.A., Lu, L.Z., 2000a. Metamorphism of basement rocks in the Central Zone of the North China Craton: implications for Paleoproterozoic tectonic evolution. Precambrian Research 103, 55–88.

Zhao, G.C., Wilde, S.A., Cawood, P.A., Lu, L.Z., 2000b. Petrology and P–T path of the Fuping mafic granulites: implications for tectonic evolution of the central zone of the North China Craton. Journal of Metamorphic Geology 18, 375–391.

Zhao, G.C., 2001. Palaeoproterozoic assembly of the North China Craton. Geological Magazine 138, 87–91.

Zhao, G.C., Wilde, S.A., Cawood, P.A., Sun, M., 2001a. Archean blocks and their boundaries in the North China Craton: lithological, geochemical, structural and P–T path constraints and tectonic evolution. Precambrian Research 107, 45–73.

Zhao, G.C., Cawood, P.A., Wilde, S.A., Lu, L.Z., 2001b. High-pressure granulites (retrograded eclogites) from the Hengshan Complex, North China Craton: petrology and tectonic implications. Journal of Petrology 42, 1141–1170.

Zhao, G.C., Wilde, S.A., Cawood, P.A., Sun, M., 2002. SHRIMP U–Pb zircon ages of the Fuping Complex: implications for accretion and assembly of the North China Craton. American Journal of Science 302, 191–226.

Zhao, G.C., Sun, M., Wilde, S.A., Li, S.Z., 2005. Late Archean to Palaeoproterozoic evolution of the North China Craton: key issues revisited. Precambrian Research 136, 177–202.

Zhao, G.C., Kröner, A., Wilde, S.A., Sun, M., Li, S.Z., Li, X.P., Zhang, J., Xia, X.P., He, Y.H., 2007. Lithotectonic elements and geological events in the Hengshan–Wutai–Fuping belt: a synthesis and implications for the evolution of the Trans-North China Orogen. Geological Magazine 144, 753–775.

Ziegler, P.A., Cloetingh, S., van Wees, J.-D., 1995. Dynamics of intra-plate compressional deformation: the Alpine foreland and other examples. Tectonophysics 252, 7–59.

Ziegler, P.A., van Wees, J.-D., Cloetingh, S., 1998. Mechanical controls on collision-related compressional intraplate deformation. Tectonophysics 300, 103–129.